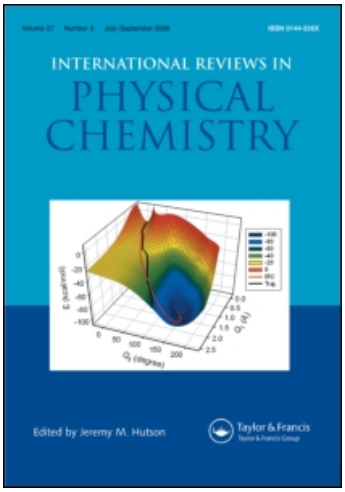

International Reviews in Physical Chemistry
Publication details, including instructions for authors and subscription information:
http://www.informaworld.com/smpp/title~content=t713724383

Collisional quenching of molecular ro-vibrational energy by He buffer loading at ultralow energies

Enrico Bodo[a]; Franco A. Gianturco[a]
[a] Department of Chemistry and CNISM, The University of Rome La Sapienza, Piazzale A. Moro 5, 00185 Rome, Italy

To cite this Article Bodo, Enrico and Gianturco, Franco A.(2006) 'Collisional quenching of molecular ro-vibrational energy by He buffer loading at ultralow energies', International Reviews in Physical Chemistry, 25: 3, 313 — 351
To link to this Article: DOI: 10.1080/01442350600772928
URL: http://dx.doi.org/10.1080/01442350600772928

International Reviews in Physical Chemistry,
Vol. 25, No. 3, July–September 2006, 313–351

Taylor & Francis
Taylor & Francis Group

Collisional quenching of molecular ro-vibrational energy by He buffer loading at ultralow energies†

ENRICO BODO and FRANCO A. GIANTURCO*

Department of Chemistry and CNISM, The University of Rome La Sapienza,
Piazzale A. Moro 5, 00185 Rome, Italy

(*Received 31 March 2005*)

In the present review we summarize in some detail the ample theoretical literature which has discussed over the last few years the computational treatment of collisionally inelastic processes at ultralow temperatures. The analysis is centred on the *ab initio* quantum treatment of collisional quenching of ro-vibrational states of simple diatomics, neutral and ionic, polar and homonuclear, interacting with a helium buffer gas. Several specific examples are analysed and their features are linked with both the details of their interaction potential energy surfaces and the special behavior of ultralow energy quantum dynamics.

Contents

*Corresponding author. Email: fa.gianturco@caspur.it; fax: +39-06-49913305
†This work is affectionately dedicated to the late Roger Miller, a brilliant scientist and a dear friend whose early departure has left a great void in our midst.

International Reviews in Physical Chemistry
ISSN 0144–235X print/ISSN 1366–591X online
http://www.tandf.co.uk/journals
DOI: 10.1080/01442350600772928

1. Introduction

Low temperature measurements of rate coefficients of various chemical processes such as simple collisional decay or even exothermic chemical reactions have always been extremely difficult to obtain especially for temperatures below 1–10 K. With the development of techniques for trapping molecules at ultracold temperatures [1–7], the construction of slowly moving crossed molecular beams [8, 9] and the creation of molecular Bose–Einstein condensates [10–16], it has become possible to explore experimentally a regime in which the kinetic energy is very low (10^{-9}–10^{-1} K) and where the scattering is determined by collisions in which the orbital angular momentum of nuclear motion in the entrance channel is zero: collisions at low and ultralow energies would indeed allow a better control of the chemical reactions and of the scattering in general [17]. Low energy collisions would also allow the exploration of a collisional regime in which the scattering is extremely sensitive to the fine details of the interaction potentials such as the weak long-range electrostatic forces between polar molecules.

Although cooling molecules is much more complicated than cooling atomic species [7, 17], a variety of methods have been proposed and implemented. 'Direct' methods are those based on cooling preexisting molecules: most prominently buffer-gas cooling [18, 19] and Stark deceleration [6, 20, 21]. In these experiments one usually begins with relatively hot molecules, typically from a molecular beam source or from laser ablation, and employs some combination of slowing, cooling and trapping. The advantage of the direct approach is mainly its wide applicability and its large yields: CaH [19, 22], PbO [23], NH [24, 25] and CaF [25, 26] have been successfully trapped and a notable variety of dipolar molecules have been slowed in beams using Stark deceleration. The main drawback is that these methods generally do not reach immediately the ultralow translational regime below 100 mK needed for the above studies, although a variety of proposals on how to do this, including evaporative cooling, already exists.

Indirect methods such as photoassociation (see for example the reviews in [27–29]) are instead a way to take advantage of the success of laser cooling in atoms: ultracold molecules are formed directly from ultracold atoms. The resulting molecules are translationally ultracold: evaporative cooling, trapping and challenges associated with them, are therefore completely circumvented. However, the method has a significant limitation on the nature of the molecular species that it can handle: presently photoassociation is limited to alkali metal diatoms only. Another indirect method of creating ultracold molecules is based on Feshbach resonances and has been realized recently [10–16]. The method relies on the adiabatic passage through a magnetically-tunable scattering resonance between two atoms and one of their molecular states. The molecules, although produced in highly excited vibrational states, have

surprisingly long lifetimes of up to 1 sec, which allows for the formation of molecular BEC through evaporative cooling. The method produces comparatively large numbers of ultracold molecules, but is limited to alkali metal dimers, and the production of vibrationally cold molecules is still an open problem.

As we have said above, one of the most interesting questions from the theoretical point of view is that the experimental analysis of the low energy collision process allows for a detailed investigation of the fine details of the Potential Energy Surfaces (PESs) once a suitable set of observables is produced and compared with theoretical predictions: the rate coefficients for various dynamical processes are some of these observables and, depending on the scheme used to produce a cold ensemble of molecules, there exist different processes that are amenable to experimental measurements.

In the case of the association of two alkali metal atoms (via photoassociation or by Feshbach resonances) the molecules are often formed in vibrationally excited states and the instability of the resulting molecular ensemble is chiefly due to vibrational de-excitation processes [30]: it therefore becomes possible to measure the overall de-excitation rate for a molecule in a well-defined vibrational state. The de-excitation process involves the collision between three identical alkali metal atoms (attempts are currently in progress to produce collision in heteronuclear molecules, see for example [31]) and during the collision a chemical exchange reaction can take place because, in the case of alkali metal atoms, there is no barrier to the atom exchange [32, 33]). The theoretical description of the resulting collision process is therefore very complex and requires a full reactive treatment. Examples of such calculations can be found in [34–36]. Despite the improvements in the experimental methods outlined above, only very new experiments with direct measurement of a vibrational quenching cross-section at ultralow energy have been reported by Weidemüller [37] and Pillet [38] who have independently measured the rate of vibrational de-excitation for Cs_2 from highly vibrational states in collision with Cs atoms and found that these rates did not depend much upon the initial vibrational state of the molecule. For example in [37] the inelastic rate coefficients for both $Cs_2(v = 32–47)$ and $Cs_2(v = 4–6)$ remain near to $1 \cdot 10^{-10}\,cm^3\,s^{-1}$. On the other hand a coefficient of about $2.5 \cdot 10^{-11}\,cm^3\,s^{-1}$ has been reported in [38] for a similar transition: the difference is probably due to the different temperature of the molecular ensemble.

By using 'direct' methods like Stark deceleration techniques [6] one can directly access ground state molecules and therefore take advantage of the production of slowly moving molecular beams [8, 9] in order to measure low energy collision processes such as exothermic chemical reactions (see for example [39] for a discussion of an interesting case). Very recently a beam experiment on cold collisions between NH and Xe atoms has been attempted and, albeit preliminarily, theoretically analyzed [40].

Buffer-gas cooling [18, 19] is a versatile technique which allows us to cool any molecule (or atom) to temperatures of a few hundred millikelvin, the temperature being determined by the equilibrium vapour pressure of the He buffer gas that is used to thermalize the molecules via elastic collisions. In this method, the trapping efficiency depends critically on the rate constants for Zeeman depolarization processes [41]: molecules are trapped in their low-field-seeking state, which generally is the Zeeman level with the highest energy, and therefore the efficiency of trapping is determined

by the ratio of the rate constants for elastic scattering and Zeeman relaxation collisions with He atoms. The thermalization of the rotational levels of the molecules occurs at a rate which is usually comparable to the rate for the cooling of the translational motion, and the vast majority of trapped molecules are in their rotational ground state. The thermalization of the vibrational levels is instead much slower. The inelastic and elastic rate constants of molecules in He buffer gas were measured in three different experiments: in the CaH experiment [22] the elastic cross-section detected at $\sim$400 mK was $\sigma^{el} = (1.5 \pm 0.6) \times 10^2$ Å^2. Due to the large rotational constant of the CaH molecule, however, no rotationally excited molecules were seen and an upper limit on the rotational temperature of $T < 2$ K was determined. The corresponding thermalization of the rotational degree of freedom was too fast to be observed producing a lower limit of the rotational inelastic quenching rate $\Gamma_{rot} \geq 10^{-15}$ cm^3 s^{-1}. After the initial laser ablation of the CaH source, vibrationally excited ($v = 1$) molecules were detected and an upper limit on the vibrational relaxation rate coefficient of the $v = 1$ state was determined: $\Gamma_{vib} < 10^{-16}$ cm^3 s^{-1} for collision with ^{3}He. For a comparison between experiments and theory see [42, 43]. The experiments with NH [25] have also provided an elastic cross-section of $\sigma^{el} = 15.0$ Å^2. The rotational temperature was also determined and the upper limit was $T < 8$ K and therefore the rotational distribution was seen to rapidly come into equilibrium with the helium buffer temperature. In the CaF case [25] the rotational temperature was determined by measuring the populations of $N = 0$ and $N = 1$ rotational states: the rotational thermalization rate turned out to be $\Gamma_{rot} \geq 2.1 \times 10^{-15}$ cm^3 s^{-1} which gave a lower limit to the rotational inelastic cross-section in the collisions of CaF with ^{3}He: $\sigma^{in} > 1.7 \times 10^{-3}$ Å^2 at $\sim$1 cm^{-1} of collision energy.

Attempts at measuring the rotational and vibrational quenching rates in molecular collision processes may also be performed using Coulomb crystals [44], where an array of trapped atomic ions or sympathetically cooled molecular ions [45–47] can be used as a cold target buffer. Indeed, the ions may represent an ideal target for molecular physics studies especially because of their low translational temperatures ($\sim$10 mK) and their strong spatial localization [44, 48]. Although less explored than neutral–neutral collision processes, collisions in ionic systems do present some important features: for example, the presence of long-range potentials may alter the threshold behavior of elastic and inelastic cross-sections [49]. Much interest is also devoted to the problem of cold ensembles of molecules with large electric dipole moments: the dipoles produce a strong long-range interparticle interaction that can be exploited for quantum computing or as a source for direct BCS pairing (e.g. see [50]). Ionic systems present the same kind of anisotropic long-range interactions and therefore may serve as an additional tool to explore the unusual properties of scattering under these conditions.

The production of cold molecules has led chemists to ask the following questions: what is the efficiency of chemical reactions and inelastic energy transfer in molecular collisions at such low temperatures? Are chemical reactions possible when the temperature approaches zero? The main goal of this article is to review part of the recent theoretical work which aims to answer these questions: in the present effort we will limit ourselves to discussing the case of inelastic scattering processes, leaving the problem of reactive scattering processes to others.

2. The theoretical machinery

Coupled differential or integrodifferential equations arise naturally in the quantum mechanical, time-independent formulation of the inelastic and reactive scattering processes whenever one looks for the time-independent scattering eigenstates of a system, here denoted as $\Psi^{i,+}$. For weakly interacting species this state is usually expanded in terms of diabatic target eigenstates:

$$\Psi^{i,+}(\mathbf{R},\mathbf{x}) = \sum_f F_{i\to f}(\mathbf{R}) X_f(\mathbf{x}) \tag{1}$$

where i labels the (collective) initial state of the colliding partners and the X_f are the eigenstates of the isolated molecules (channel eigenstates) with internal coordinates denoted by $\mathbf{x}$. The $F_{i\to f}$ are the channel components of the scattering wavefunction that depend on the interparticle distance $\mathbf{R}$ and which have to be determined by solving the Schrödinger equation subject to the usual boundary conditions

$$F_{i\to f}(\mathbf{R}) \to \delta_{ij} h^{(-)}(\mathbf{R}) - S_{fi} h^{(+)}(\mathbf{R}) \quad \text{as } R \to \infty \tag{2}$$

where f denotes a channel which is asymptotically accessible at the selected energy (open channel) and $h^{(\pm)}$ is a pair of linearly independent free-particle solutions. In the absence of a magnetic or electric field, the total angular momentum is a constant of the motion and one can thus consider a single angular momentum J at a time: when $h^{(\pm)}$ are chosen to be the appropriate Riccati–Hankel functions the coefficients S_{fi} are the elements of the partial wave scattering matrix, often denoted as S^J. In the presence of an external field the situation is more complex and all the total angular momentum components are coupled together [41, 43]: we shall not be discussing such a case in the present review.

In principle, the sum in equation (1) should span the relevant discrete spectrum of the isolated molecules and, whenever possible, also its continuum portion. Usually, however, numerically converged scattering observables are obtained by retaining only a limited number of discrete channels. One thus gets a set of M coupled differential equations for the $F_{i\to f}$ unknowns subject to the regularity condition of each solution at the origin ($F_{i\to f}(0) = 0$) and to the boundary conditions given by equation (2).

These radial functions which form a matrix solution $\boldsymbol{\psi}$ appear in the familiar set of coupled, second order homogeneous differential equations:

$$\left\{ \frac{d^2}{dR^2} + \mathbf{k}^2 - \mathbf{V}(R) - \frac{\mathbf{l}^2}{R^2} \right\} \boldsymbol{\psi} = 0 \tag{3}$$

where $[\mathbf{k}^2]_{ij} = \delta_{ij} 2\mu(E - \epsilon_i)$ is the diagonal matrix of the asymptotic (squared) wavevectors and $[\mathbf{l}^2]_{ij} = \delta_{ij} l_i(l_i + 1)$ is the matrix representation of the square of the orbital angular momentum operator. Finally $\mathbf{V}(R) = 2\mu\mathbf{U}(R)$ is the potential coupling matrix which is given by different expressions depending on the angular

momenta involved. In the case of a molecule in its singlet electronic spin state interacting with a structureless atom the expression is simple and is given by

$$[\mathbf{U}^J(R)]_{jl,j'l'} = \sum_{\lambda} f_\lambda(l'j';l''j'';J)V_\lambda(R) \tag{4}$$

where the $f_\lambda(l'j';l''j'';J)$ are the well-known coefficients of Percival and Seaton [51], j and j' are the initial and final molecular rotational quantum numbers and $V_\lambda(R)$ are the Legendre expansion coefficients of the potential.

The simulation of inelastic collisions involving open-shell diatomic molecules or atoms is more complicated because the relative translational motion can couple not only to the rotational motion of the molecule but also with the internal electronic angular momenta (if any) and the various spin momenta as well. For example when we have a $^2\Pi$ molecule in collision with a structureless atom, the cylindrical degeneracy of the Π electronic state is lifted and therefore the description of the collisional process now involves two electronic potential energy surfaces, corresponding to the two states of A' and A'' symmetry (see [52–54] for further details).

One usually does not solve directly for $\boldsymbol{\psi}$ but defines a Log-Derivative matrix $\mathbf{Y} = \boldsymbol{\psi}'\boldsymbol{\psi}^{-1}$ which satisfies the Riccati equation

$$\frac{d\mathbf{Y}}{dR} + \mathbf{W}(R) + \mathbf{Y}^2 = 0 \tag{5}$$

with $\mathbf{W}(R) = \mathbf{k}^2 - \mathbf{V}(R) - \mathbf{l}^2/R^2$ and solves the latter equation which avoids the need to stabilize the wavefunction against linear dependence of the solution vectors. Beginning with the condition $\mathbf{Y}^{-1} = 0$, one usually employs a propagator such as the Log-Derivative propagator [55] and obtains the scattering observables in the asymptotic region at $R_{\max}$ where the solution matrix can be written in the form

$$\Psi(R_{\max}) = \mathbf{J}(R_{\max}) - \mathbf{N}(R_{\max})\,\mathbf{K} \tag{6}$$

with $\mathbf{J}(R_{\max})$ and $\mathbf{N}(R_{\max})$ diagonal matrices of Riccati–Bessel and Riccati–Neumann functions. The $\mathbf{K}$ matrix defines a set of mixing coefficients of the free-particle solutions and is related to the S-matrix by a simple transformation. Therefore, at the end of the propagation one uses the Log-Derivative matrix to obtain the $\mathbf{K}$ matrix by solving the following linear system (with $\mathbf{J}$, $\mathbf{N}$ and their derivatives evaluated at $R_{\max}$)

$$(\mathbf{N}' - \mathbf{Y}\,\mathbf{N})\,\mathbf{K} = \mathbf{J}' - \mathbf{Y}\,\mathbf{J}. \tag{7}$$

Starting with the above prescription, we have implemented a new algorithm based on the multichannel variable phase equation [56] which is particularly useful in the presence of long-range potentials [57].

When no electric and magnetic fields are present the total angular momentum is a constant of the motion and therefore one performs separate calculations for each J value. Given a certain initial molecular total angular momentum N, the s-wave

calculation with $l=0$ is given for total angular momentum value $J=N$. The details of the numerical implementation of the close coupling scheme obviously depend on the specific values of the spin and other angular momenta involved in the collision processes. In general terms, however, the total quenching cross-section for a molecule which initially is in the (v, N) ro-vibrational state is obtained as a sum over the various total angular momenta of the relevant T-matrix elements

$$\sigma(v, N \rightarrow v', N', E_i) = \frac{\pi}{(2N+1)k^2_{v,N}} \sum_J (2J+1) \sum_{l=|J-N|}^{J+N} \sum_{l'=|J-N'|}^{J+N'} \left| T^J_{vNl \rightarrow v'N'l'} \right|^2 \qquad (8)$$

2.1. *Zeeman depolarization*

As we have already pointed out above, the efficiency of the buffer gas loading technique depends on the rate at which collisions with He atoms induce relaxation from the Zeeman level with the highest energy which generally is the only level that can be trapped. In order to estimate the rates for Zeeman depolarization, and therefore the possibility of cooling a molecular species using buffer gas loading technique, it is necessary to perform the calculation taking into account the external magnetic field. When an external field is present there are several complications in the scheme outlined above: first the total angular momentum of the system is not a constant of motion anymore and all its values are coupled together. Further new terms appears in the Hamiltonian which represent the interaction of the two colliding partners with the field and depend on the spins of the two partners. Krems *et al.* [41] have suggested to expand the total wavefunction in products of eigenfunctions of $\mathbf{I}^2$, of the isolated molecule Hamiltonian and of the two spins operators. The actual expansions depend on the nature of the colliding partners and we defer the interested reader to [17, 41] for further details. We limit ourselves here to pointing out a remarkable property of Zeeman relaxation: the mechanism driving Zeeman transitions in rotationally ground state molecules depends on the spin multiplicity of the electronic state: in $^2\Sigma$ molecules the coupling between the Zeeman sublevels comes from the spin-rotation interaction $H_{\mathrm{sr}} = \gamma_0 \mathbf{j} \cdot \mathbf{S}$ and the Zeeman transitions must take place through a three-step mechanism involving a rotationally excited state. On the other hand, the Zeeman sublevels in $^3\Sigma$ molecules are coupled directly by the spin–spin interaction in the Hamiltonian which then mixes the rotational levels with $N=0$ and $N=2$. Therefore, the rate of the Zeeman relaxation in both doublet and triplet molecules depends on their rotational constant B. The cross-section for Zeeman depolarization is approximately proportional to $1/B^2$ for the triplet molecule and to $1/B^4$ for the doublet molecule. Other studies of Zeeman depolarization can be found in [58–60].

2.2. *Ultralow energy collisions*

When the collision energy becomes very low the scattering problem is partly simplified. In 1948 Wigner obtained a general expression for the energy dependence of cross-sections near threshold for elastic and inelastic collision processes [61] which is generally referred to as the Wigner's threshold law. Given a particle in a well-defined

initial quantum state j and a collider at very low energy with relative angular momentum l we can have only two kinds of processes: an elastic collision in which the internal state of the particle does not change and an inelastic collision in which the particle relaxes to a lower quantum level f. The dependence of the cross-sections on the initial relative velocities v_j is given by

$$\begin{aligned} \sigma_j^{\mathrm{el}} &\sim v_j^{4l} \\ \sigma_j^{\mathrm{in}} &\sim v_j^{2l-1} \end{aligned} \tag{9}$$

where j identifies the initial state of the particle and where the total quenching cross-section σ^{in} is a sum over all the state-to-state cross-sections to all the accessible channels with $E_f < E_j$:

$$\sigma_j(E_j) = \sum_f \sigma(j \to f, E_j). \tag{10}$$

Therefore, when the initial relative velocity goes to zero all the $l \neq 0$ partial waves stop contributing to the scattering and one reaches the s-wave regime in which it is possible to define a complex scattering length $a_j = \alpha_j - i\beta_j$ [62]. The parameters α_j and β_j are related to the elastic S-matrix element $S_{jj}(k_j)$ as $k_j \to 0$ according to:

$$\begin{aligned} \alpha_j &= \lim_{k_j \to 0} -\frac{\Im(S_{jj}^{\mathrm{el}})}{2k_j} \\ \beta_j &= \lim_{k_j \to 0} \frac{1 - \Re(S_{jj}^{\mathrm{el}})}{2k_j}. \end{aligned} \tag{11}$$

The elastic and total inelastic scattering cross-sections at zero energy are hence given by

$$\sigma_j^{\mathrm{el}} = 4\pi |a_j|^2; \quad \sigma_j^{\mathrm{in}} = \frac{4\pi\beta_j}{k_j}. \tag{12}$$

For small values of k_j the poles of the S-matrix can then be further located by the relation [62]:

$$E_p = \frac{k_p^2}{2\mu} = -\frac{\cos 2\gamma_j + i \sin 2\gamma_j}{2\mu |a_j|^2} = E_j' - \frac{i}{2}\Gamma_j \tag{13}$$

where $\gamma_j = \arctan(\beta_j/\alpha_j)$, μ is the reduced mass and Γ_j the width of the resonance associated with the pole. If $\alpha_j > 0$ the real part of E_p is the binding energy of the least bound resonance and if $\alpha_j < 0$ it is the energy of the virtual state of least energy. The lifetime τ_j and width Γ_j of the resonance are given by

$$\tau_j = \frac{1}{|\Gamma_j|} = \frac{\mu |a_j|^4}{2|\alpha_j|\beta_j} \tag{14}$$

The imaginary part of the scattering length, as we reported in equation (12), is related to the total inelastic quenching cross-section in the limit of zero velocity. It is possible to show that expression (12) gives a zero temperature rate constant

$$R_j(T \to 0) = \frac{4\pi\hbar\beta_j}{\mu} \tag{15}$$

The zero temperature limit of the quenching rate coefficient is finite because, according to Wigner's law the quenching cross-section varies inversely with the velocity as the kinetic energy approaches zero. The quenching rate coefficients at other temperatures are obtained by averaging the cross-sections over a Boltzmann distribution of velocities of the incoming atom at a specified temperature T:

$$R_j(T) = \left(\frac{8k_BT}{\pi\mu}\right)\int_0^\infty \sigma_j^{\text{in}}(E)\exp(-E/k_BT)EdE \tag{16}$$

where k_B is the Boltzmann constant.

From the theoretical point of view, making precise predictions for ultralow energy collisions is extremely difficult because of the sensitivity of the results to the details of the PES and especially to the long-range tail of it. The C_6 and higher order coefficients are rarely known from theoretical predictions and uncertainties in those quantities of 10% may cause variation of orders of magnitude in the cross-sections: as an example we report in figure 1 a model calculation by Balakrishnan et al. [63] in which we can see the huge variation of the total vibrational quenching cross-section for the $H_2(v, j = 0)$+He system when the long-range part of the potential is omitted. Another example of a study which analyzed the sensitivity of the calculated cross-sections with respect to small variations of the potential has been presented by Quéméner *et al.* in [64]. In particular the sensitivity of these quantities on the three-body interaction has been performed: cross-sections, rate coefficients and scattering lengths are very sensitive to three-body effects.

3. Rotational quenching

Rotational de-excitation processes at ultralow energies depend mainly on two features of the potential energy surface: the angular anisotropy at short range and the presence of a long-range anisotropic tail. In neutral systems the latter is generally not present because the long-range coefficients C_6 and C_8 are nearly isotropic especially for molecules with relatively short bond distances like H_2 and CO. For ionic systems one can have instead long-range anisotropic contributions: for example we have analyzed the OH^--He system (see below) where the long-range potential is given by

$$V_{\text{LR}}(R) \sim -\frac{\alpha(\text{He})}{2R^4} - \frac{2\alpha(\text{He})\mu(\text{OH}^-)}{R^5}\cos\theta \tag{17}$$

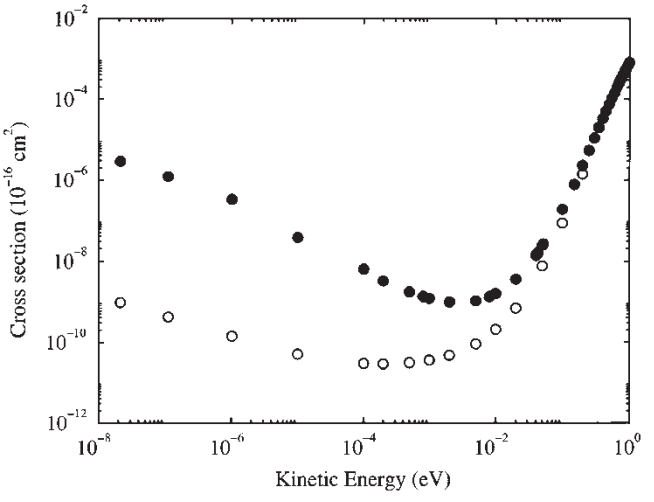

Figure 1. Exothermic vibrational relaxation cross-section for $^4He + H_2$ collisions as a function of kinetic energy. Filled circles are the results obtained using the full interaction potential and the open circles are the results obtained from a calculation in which the long-range part of the potential is omitted. Adapted from [63].

where α is the He polarizability, μ is the OH^- dipole moment and R and θ are the usual atom–molecule Jacobi coordinates. The second term on the r.h.s. clearly depends on the $P_1(\cos\theta)$ Legendre polynomial and therefore strongly couples the $\Delta j = 1$ transitions. For neutral molecules, rotational quenching in a cold buffer gas is very efficient. As it has also been seen in various experiments [19, 22, 23, 25, 26], most of rotationally excited molecules when in contact with a cold buffer gas of He atoms thermalize very rapidly to its low temperature (< 10 K) so that, unless the rotational spacing is extremely low, there is no substantial population left in the rotationally excited states. The rate of the de-excitation process is so fast that it turns out to be very difficult to monitor the population of the rotationally excited states as the system quenches to its ground state.

3.1. *Neutral systems with closed-shell molecules*

Despite the efficiency of the process, the issue of the possible stability of rotationally hot molecules in a cold buffer gas has been explored in rigorous calculations of atom–molecule collisions at ultracold temperatures in various papers [65, 66]: it has been predicted there that hydrogen 'super rotors' in certain states may experience virtually no collisional quenching at all [65, 66]. In general as the rotational level of the molecule increases, the energy gap for pure rotational transitions also increases, and the efficiency of rotational quenching decreases. However, although the fate of the rotationally excited molecule depends on its initial ro-vibrational state it also depends on whether or not a nearby quasiresonant vibration–rotation transition (QRVR) [67] is energetically allowed. If v and j are the vibrational and rotational

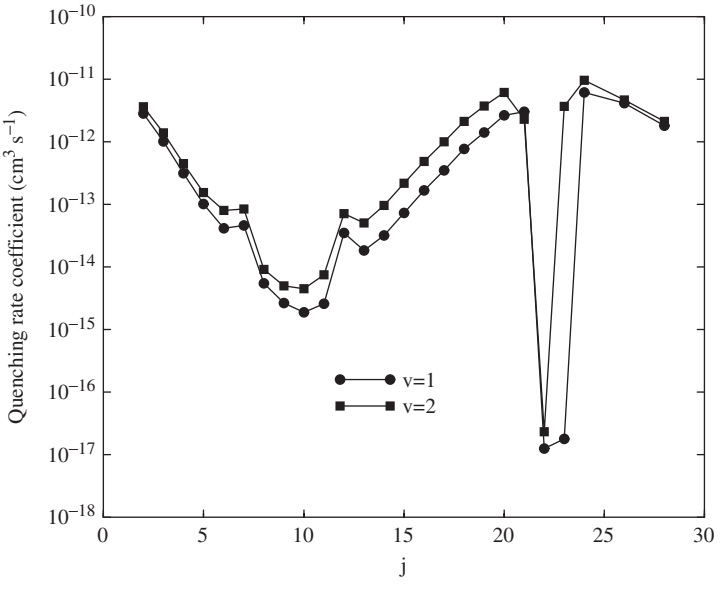

Figure 2. Quenching rate coefficients for collisions of ^{4}He with $H_2(v, j)$ in the limit of zero temperature. The rate coefficients include contributions from all possible de-excitation channels. Adapted from [66].

quantum numbers of the diatom, then the general propensity rule followed by QRVR transitions is [67]

$$\Delta j = -n\Delta v \tag{18}$$

where n is a small integer. This happens when the vibrational and rotational motion are approximately in resonance and an integral number of complete vibrations will occur during each half rotation. The presence of a QRVR condition together with an ultralow collision energy in the entrance channel can produce sharp structures in the rotational distributions of the total quenching rate coefficients: as an example, we report in figure 2 the total quenching rate of highly rotationally excited H_2 molecules in collision with ^{4}He. Specific rotationally hot molecules are stable against cold collisions, as the internal energy loss rate is dramatically reduced with respect to neighboring energy levels. The rate coefficients for He-H_2 collisions suggest that it may be possible to maintain a large density of molecules for these values of j before ultimately losing them to collisional or radioactive decay. The above numerical experiment has also been repeated with oxygen molecule [68], but the quenching efficiency for rotational transitions was found to be larger for oxygen than for H_2, therefore indicating that the near-dissociation dynamics of molecular oxygen would be less interesting and probably more difficult to study experimentally.

We have further looked at the efficiency of rotational quenching in very weakly interacting systems using the $Li_2 + He$ system as a prototype [69]. The interaction of He with the Li_2 molecule in its singlet state is extremely weak and presents a collinear

minimum of less than one wavenumber unable to produce even a weak bound state [70]. The PES has been computed in Jacobi coordinates fixing the internuclear distance of the Li_2 molecule at its equilibrium value of 2.7 Å and using the QCISD(T) method with a cc-pvQZ basis set. Each of the calculated points has been counterpoise corrected to avoid the BSSE errors that in this system turn out to be very large. More details on the *ab initio* results as well as the specific form of the analytical fitting of the PES employed here can be found in [69]. The produced molecular interaction turns out to be essentially isotropic a feature that was indeed important for the analysis of the rotational de-excitation collisions where we found that the computed energy transfer probabilities suggested a marked inefficiency of the collisional cooling mechanism. To get a more precise idea on the global behavior of this new PES we also report a 3D view of it in figure 3. In that picture one easily notices the chiefly

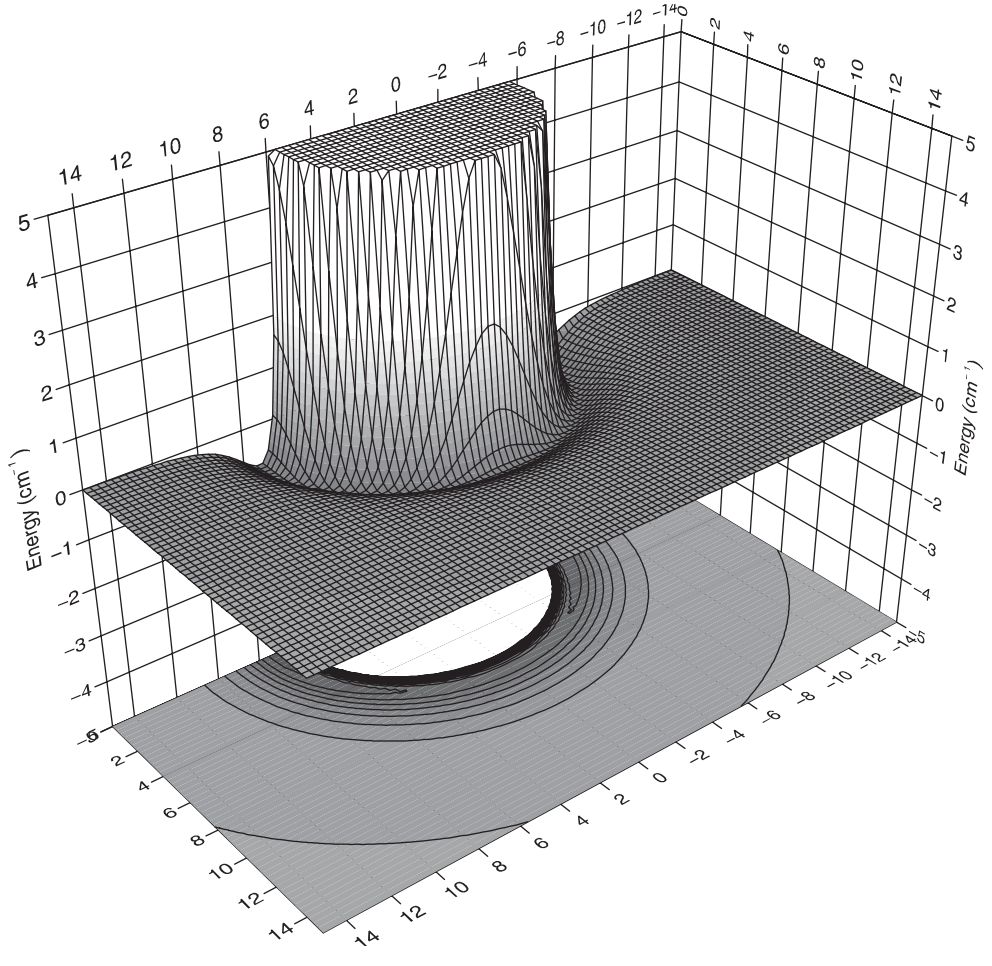

Figure 3. 3D view of the interaction potential. Energies in cm^{-1} and distances in Å. Adapted from [70].

isotropic shape of the interaction and the well-defined molecular core containing the Li_2 partner, identified by the repulsive region which gives negligible indication of any orientation-dependent molecular feature.

Rotationally elastic and inelastic cross-sections have been calculated and their ultralow energy behavior is reported in figure 4: the top left panel shows elastic cross-sections for various initial j levels of the molecule: the four cross-sections are very similar to each other (see also [71] for a similar result in O_2+He collisions). The weakness of the interaction potential makes the cross-sections very smooth and without any sign of resonances even for energies larger than $1\,cm^{-1}$ where centrifugal barriers often induce shape resonances. Since the interaction potential is so weak, the scattering is largely determined by the presence of a virtual state at $-0.3\ cm^{-2}$. The various inelastic cross-sections are reported in the other three panels: for energies larger than $1\,cm^{-1}$ the de-excitation cross-sections are now one or two orders of magnitude smaller than the elastic ones because of the small angular anisotropy. At even smaller energies the cross-sections start to diverge following Wigner's law. Given the extremely small rotational coupling in the present complex, the de-excitation cross-section is chiefly controlled by the energy difference between the rotational levels and therefore becomes larger when the initial energy content of the molecule is higher. Considering the rotational constant of the molecule ($\sim 0.67\,cm^{-1}$), it is hard to

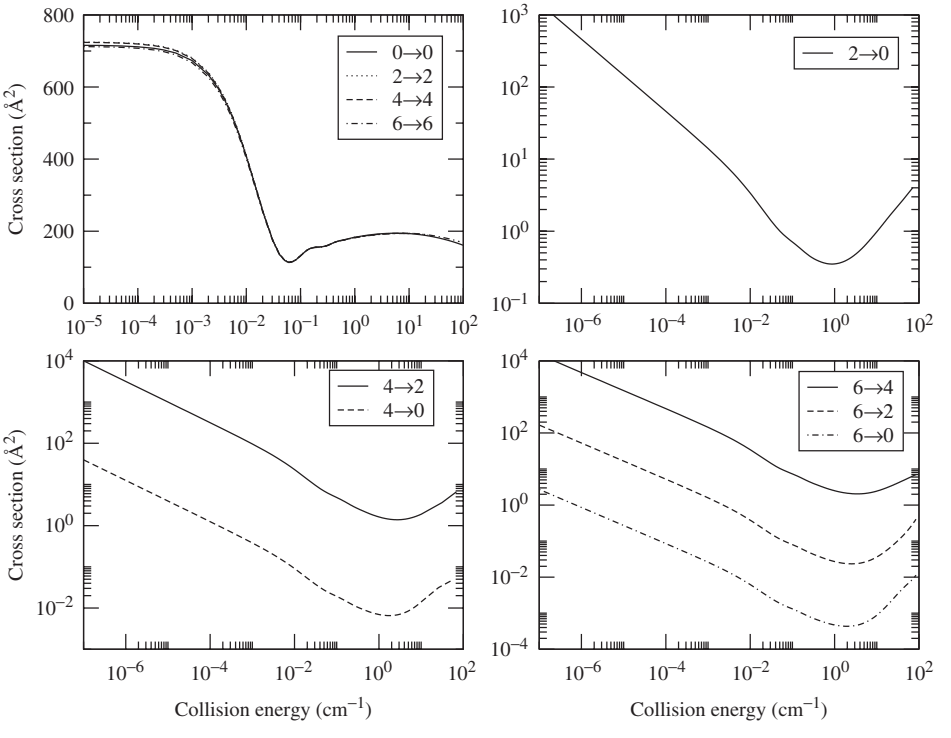

Figure 4. Rotationally elastic and inelastic cross-sections as a function of collision energy and for different initial rotational states. Adapted from [69].

say whether rotationally excited Li_2 molecules could be rapidly cooled by an He buffer gas at the energies expected to exist in the experiments [72]. The rate constants for inelastic de-excitation in this system were found to be of the order of $10^{-12}\,cm^3\,s^{-1}$ which is still three orders of magnitude larger than the lower limit found in experiments (see Introduction).

3.2. *Neutral systems with open-shell molecules*

The systems mentioned up to now were relatively simple systems in which a singlet molecule was colliding with a structureless atom. However, the species that are employed in the cryogenic traps for buffer gas loading techniques or in other experiments are often molecular species with unpaired electrons. Obviously, the collisions between an open-shell atom and and open-shell molecule are more complicated because of the new interaction terms appearing in the Hamiltonian. However various calculations have been performed: one by us on $OH(^2\Pi)$-He [73], one by Balakrishnan *et al.* on $CaH(^2\Sigma+)$-He [42] and another by Krems *et al.* on $NH(^3\Sigma-)$-He [74].

For the case of $OH(X^2\Pi)$ as a molecular target the asymptotic molecular levels are reported in figure 5 where the total angular momentum of the diatomic molecule is given by j. The Λ doublet levels are distinguished by the symmetry index ϵ which can take the value $+1$ (e-labelled levels) or -1 (f-labelled levels). The description of $OH(X^2\Pi)$ in Hund's case (a) and (b) can be found with more details in our paper [73]. In the ultracold temperature limit we know that quantum suppression requires the collision dynamics to be determined by the s-wave scattering component (i.e. $l=0$). We have carried out calculations for collision energies from $300\,cm^{-1}$ down to $10^{-5}\,cm^{-1}$, and for all initial rotational states of OH molecule represented in figure 5. As an example, figure 6 presents the cross-sections for rotational relaxation from the states of OH ($\frac{3}{2}F_2e/f$) to all the lower-lying states after collision with He.

Our results suggest that in most cases the larger integral cross-section occurs for a parity conserving transition. On the other hand, the larger integral cross-sections that correspond to spin–orbit conserving ($F_1 \to F_1$ and $F_2 \to F_2$) processes have $\Delta j = -1$ as a propensity indicator, while the spin–orbit changing transitions have $\Delta j = 1$, except for the transitions from the $F_1 7/2f+$ and $F_1 11/2f+$ states, which have $\Delta j = -2$. This is due to the dynamical tendency of the present system to minimize the energy gap between the initial and the final states. In our analysis of the present results we also found that transitions from the F_2 states are all spin–orbit changing transitions ($F_2 \to F_1$), while those from F_1 have a propensity to conserve the spin–orbit value ($F_1 \to F_1$).

It is also significant to observe the relaxation efficiency between the two nearly isoenergetic Λ doublet levels ($f \to e$) given by figure 7 where we report inelastic cross-sections at ultralow energies ($10^{-5}\,cm^{-1}$) for different symmetries and different j values. One clearly sees that the transitions within the F_1 manifold appear to be largely independent of j while the same transitions within the F_2 manifold show a marked size reduction as j increases. Thus, one can say that collisional quenching of rotationally 'hot' OH molecules would be much more efficient (i.e. will propagate well over a range of j values) if the system is in the higher Ω states typical of the F_1 symmetry.

As we have said above, other open-shell systems have been analyzed in terms of rotational de-excitation processes: Krems and coworkers report in [43] calculations for the elastic energy transfer and Zeeman relaxation in collisions of ground state NH molecules with ^{3}He atoms in a magnetic field. They employed a close coupling technique using the fully uncoupled space-fixed representation [41] to make predictions for experiments on the buffer-gas loading of NH and to establish the mechanism of Zeeman transitions in NH-He collisions. The rotational angular momentum j is not a good quantum number in $^3\Sigma$ molecules: the spin–spin interaction couples states with j and $j = j \pm 2$ and the rotational ground state is split into three Zeeman sublevels;

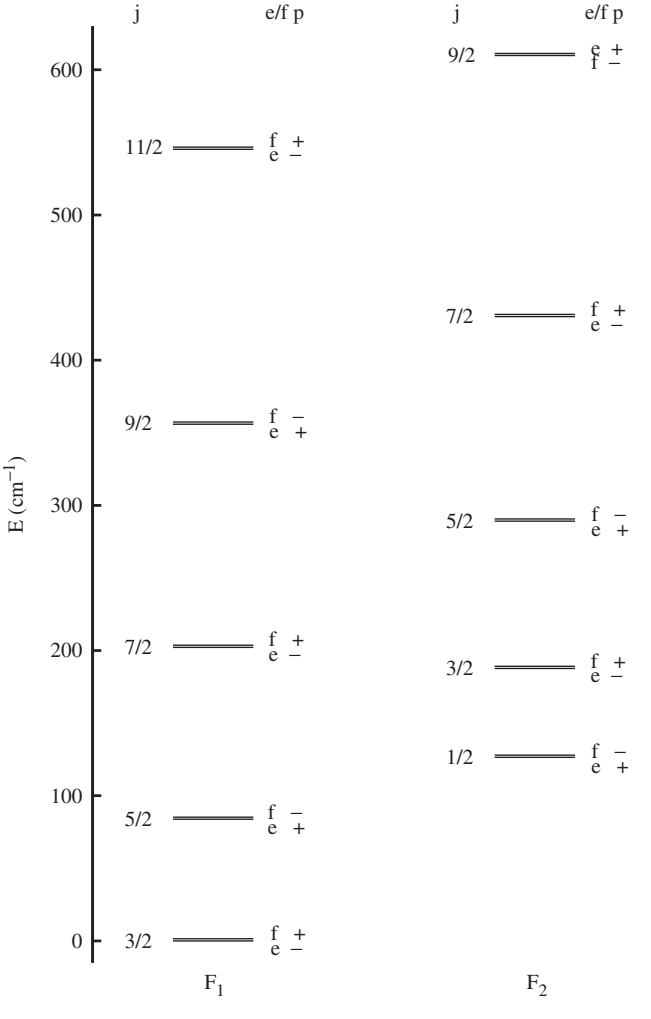

Figure 5. Energy level diagram for the lowest rotational levels of the OH ($X^2\Pi$). The energy levels are labelled by their rotational quantum number j, parity p, and Λ-doubling symmetry e/f. The spacing of the rotational levels is to scale, but the energy difference between the components of each Λ-doublet is exaggerated to improve clarity. Adapted from [73].

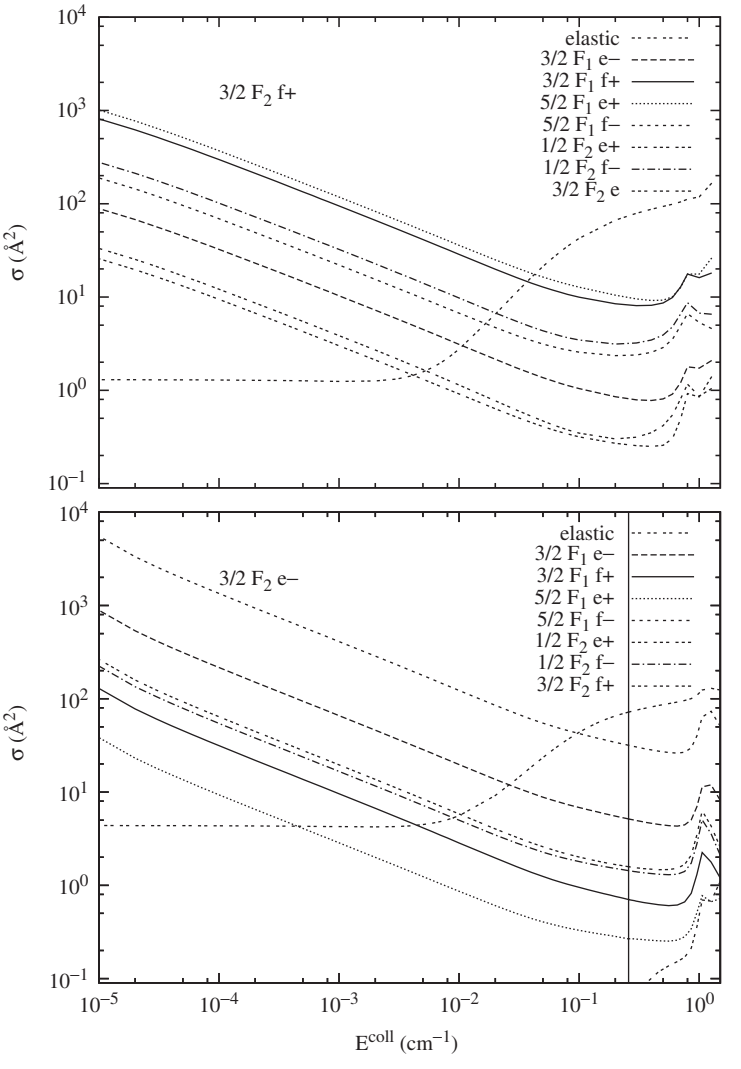

Figure 6. Computed integral cross-sections for elastic and relaxation processes to individual fine structure levels as functions of collision energy.

the state with $m_N = 1$ is trappable in a magnetic field and transitions to the states with $m_N = 0, -1$ lead to trap losses. The Zeeman relaxation in NH-He collisions in weak magnetic fields is at least five orders of magnitude slower than the elastic energy transfer which suggests that buffer-gas loading of NH molecules in a magnetic trap should be efficient. The rate constants for rotational relaxation of NH in the five excited rotational energy levels by collisions with ^{3}He at 0.5 K (see figure 11) has also been calculated. The rate for relaxation of NH($j = 1$) is $\sim 2 \times 10^{-12}$ cm^3 s^{-1}, one order of magnitude smaller than the rates for relaxation of NH in higher rotational levels.

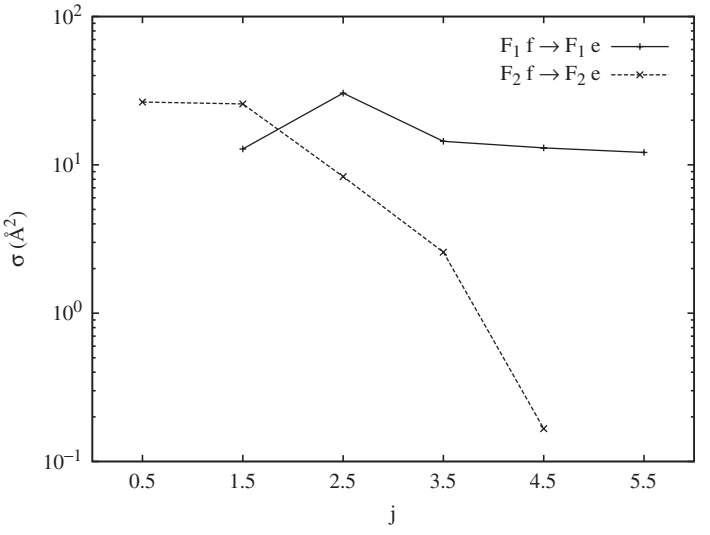

Figure 7. Computed integral inelastic cross-sections between the two nearly isoenergetic Λ doublet levels of the same j as function of the j value, at $E = 10^{-5}\,\mathrm{cm}^{-1}$.

The rotational relaxation is however so fast that most molecules in the buffer-gas experiment are predicted to be in the rotational ground state in agreement with what has been found in the experiments [25].

3.3. *Ionic systems*

More recently attention has shifted towards ionic systems where particular features of the potential may have a marked effect on the scattering observables. In general, the main feature of the PES is the presence of a long-range interaction that may be also anisotropic depending on the system at hand. As an example of such behavior, we report in figure 8 three cuts for three different PESs for the systems OH^--He [75], OH^+-He [75] and OH-He [76]. The three cuts are taken at the angular geometry for which we have the absolute minimum with the three molecules kept at their equilibrium geometries. For neutral OH the minimum geometry is bent with a Jacobi angle of $\sim 70^\circ$, for OH^+ it is collinear with the He atom sitting on the H side and for OH^- it is again collinear but with the He on the oxygen side. The dominant interaction that we obtain with the cationic species is clearly visible and we also see quite clearly the dramatic scaling of the attractive wells of the minimum energy structures when going to the neutral OH. More interesting for the present discussion is, however, the comparison of the long-range tails of the three potentials showed in the inset in figure 8: the neutral potential has a dominant long-range part which dies off quite rapidly as C_6/R^6, while the two ionic potentials show the characteristic long-range tails due to induction forces. The potential for both ionic systems is given by equation (17). Since the first term is largely

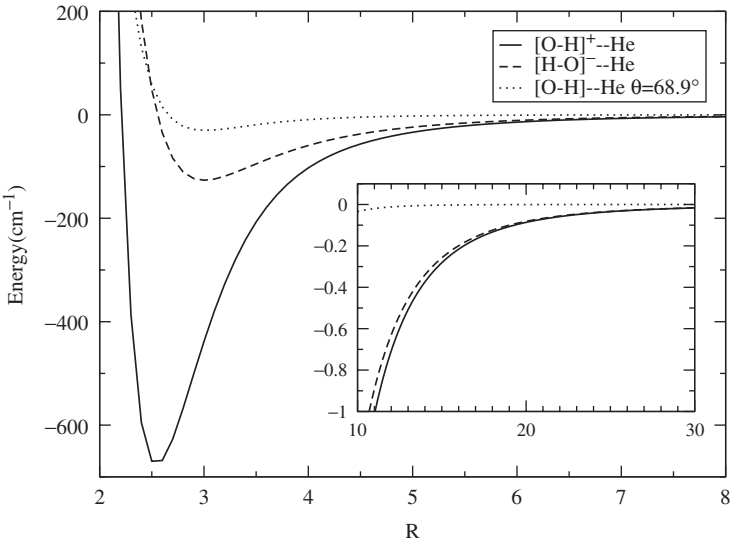

Figure 8. Computed PECs associated with the three minimum-energy configurations of the OH-He complexes for the neutral, cationic and anionic molecules. Adapted from [75].

dominant for $R > 20$ Å the two potentials for the ionic systems turn out to be very similar: the presence of a long-range isotropic term in the potential is important because it directly affects elastic scattering cross-sections and also vibrational de-excitation.

The interactions between the $OH^+(^3\Sigma^-)$ and $OH^-(^1\Sigma^-)$ with He which we show above, have been calculated in the rigid rotor approximation [75] using the MP4 approach and with the aug-cc-pVQZ basis set, including all along the BSSE corrections via the counterpoise method [77]. We further proceeded to obtain an analytic representation of both PESs by using a two-centre expansion scheme [78] whereby the long-range interaction is written as:

$$V_{\mathrm{LR}}(R,\theta) \simeq -\frac{c_4 f_4(\beta R)}{R^4} - \frac{c_5 f_5(\beta R)}{R^5}\cos\theta \tag{19}$$

where f_4 and f_5 are damping functions [79] which ensures that the asymptotic tail of the interaction has the correct behavior. By comparing this expression with that of equation (17) we can sample the quality of our *ab initio* calculations and of the fitting itself: the value for α(He) extracted from the fitting which is 1.41 and 1.55 a.u. for OH^+ and OH^- respectively is in agreement with the experimental value of 1.38 a.u. We also compared the dipoles coming out from the fitting (0.939 and 0.453 a.u.), with the *ab initio* values of them (0.849 and 0.566 a.u.). The two PESs are reported in figure 9 where we represent the potential energy isolines in the (x/y) plane of the Jacobi coordinates.

We have performed calculations for the rotational de-excitation of the $OH^-(^1\Sigma^-)$ and we have compared it to similar heteronuclear systems such as OH and NH in order to see differences due to the presence of ionic interactions. In our study we

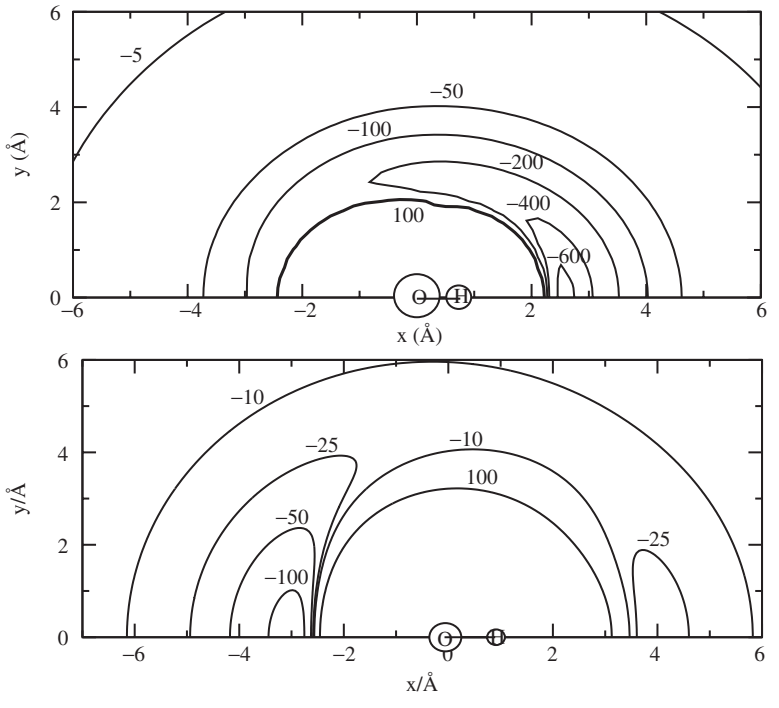

Figure 9. Rigid rotor potential for the $OH^{\pm}$-He systems. The distances are in Å and the isoline labels are energy in cm^{-1}. The molecular positions are reported at the bottom of the figure. Adapted from [75].

have used the rigid rotor approximation including 21 total angular momentum values and all the rotational states up to $j_{max} = 18$. The rotational constant of OH^- was taken to be $18.57014\,cm^{-1}$. The quenching and elastic cross-sections for the rotational transitions are reported in figure 10 for various collision energies starting from 10^{-9} up to $0.1\,cm^{-1}$. For rotational levels under $j = 4$, the cross-sections already follow the Wigner's law from energies of $\sim 10^{-4}\,cm^{-1}$, while for $j = 5$ it is valid only for energies below $10^{-6}\,cm^{-1}$. This effect is related to the appearance of a strong shape resonance due to the $l \neq 0$ components at an energy of $10^{-4}\,cm^{-1}$ for $j = 5$ which then moves gradually to higher energies for higher j values. In the case of the elastic cross-sections we can see that the cross-sections for the lowest energies are very similar for all choices of the initial rotational j states in the zero energy limit. This levelling effect of the elastic cross-section which results to be nearly independent of the initial rotational state has already been noticed by us in the $Li_2 + He$ and in O_2-He systems as pointed out in the previous section. The shape resonance which was already noticed in the inelastic cross-section is now much more evident for initial values of $j = 6 - 8$. In general we can see how the elastic cross-section is much larger ($\sim 10^4$ Å) for this ionic system with respect to what has been measured or calculated for neutral ones: for example for Li_2-He the calculated elastic cross-section was about 7×10^2 Å at $10^{-3}\,cm^{-1}$, for OH-He ~ 5 Å at the same energy. Measured values were about $\sim 1.5 \times 10^2$ and $\sim 1.5 \times 10^1$ Å for CaH and NH at energies of

about one wavenumber. Moreover Wigner's law regime is reached at a much lower energy when compared to that of OH or Li_2. These effects are obviously due to the presence of a long-range spherical interaction due to induction forces. We can also compare the rate constants for rotational quenching in this ionic system, with those obtained earlier for the He+OH/NH collision: figure 11 shows in fact the zero temperature rate constants for rotational relaxation of OH^- (solid line) and of OH (level F_2e) [73] (dashes) to all lower-lying levels. The corresponding behavior of the $NH(X^3\Sigma)$ [43] target molecule is further shown by the short dashes. The quenching rates are one order of magnitude larger than those exhibited by the neutral OH or NH partners, a result that confirms the relatively important role of the long-range

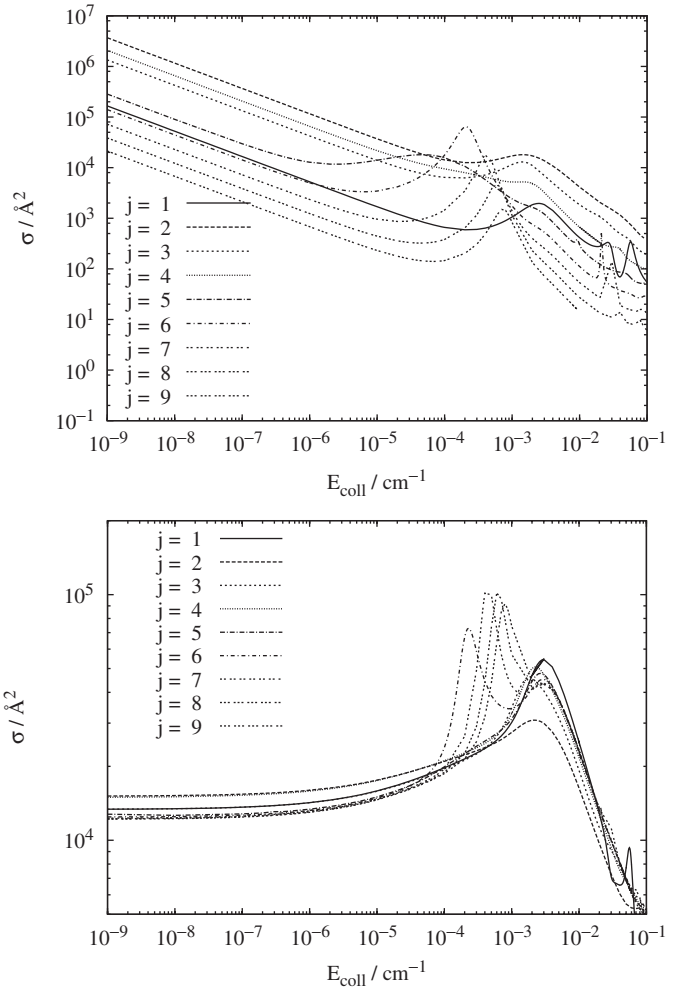

Figure 10. Quenching (upper panel) and elastic (lower panel) cross-sections for He-OH^-, inelastic transitions for different rotational j states to all lower lying final states. Adapted from [73].

behavior of the anisotropic coefficients of the interaction potential in guiding inelasticity between near-Van-der-Waals systems.

The main effect of the ionic potential in the latter system has been that of increasing the elastic cross-sections in the Wigner regime and that of reducing the collision energy at which this regime is reached. However, we have also seen that the effect on the inelastic process was rather limited. We have however met in our studies two other systems in which the presence of ionic interactions produced a much more dramatic enhancement of inelastic cross-sections. These two systems are the He_2^++He system and the analogous Ne_2^++Ne systems [81]. To see this effect more in detail we report in table 1 the values of the scattering lengths and the zero temperature rate coefficients we have calculated for collisions within those systems. We employed there the two rigid rotor (RR) potential energy surfaces (PESs) that we had calculated earlier in our group using highly correlated *ab initio* methods [82, 83]. The long-range points were fitted to the multipolar expansion for the electrostatic interactions for which we employed the experimental values of the dipole polarizabilities α of the neutral atoms (α(He) = 1.38 a.u. and α(Ne) = 2.67 a.u.). We solved the close coupled (CC) equations in the rigid rotor approximation, which excludes the possibility of vibrational transitions and reactive collisions but should yield reliable results for pure rotational transitions. For a given partial wave of angular momentum l and initial internal quantum angular number j the total angular quantum number J ranges from $|j-l|$ to $j+l$. For s-wave scattering with $l=0$, $J=j$. For the He system we employed nine rotational levels and for the Ne system 32 with 10 partial waves for both. We present in table 1 the real and imaginary parts of the scattering lengths together with the limiting values of the rate constants for the quenching process. The real parts of the scattering lengths are very large determining the sizes of the elastic cross-sections

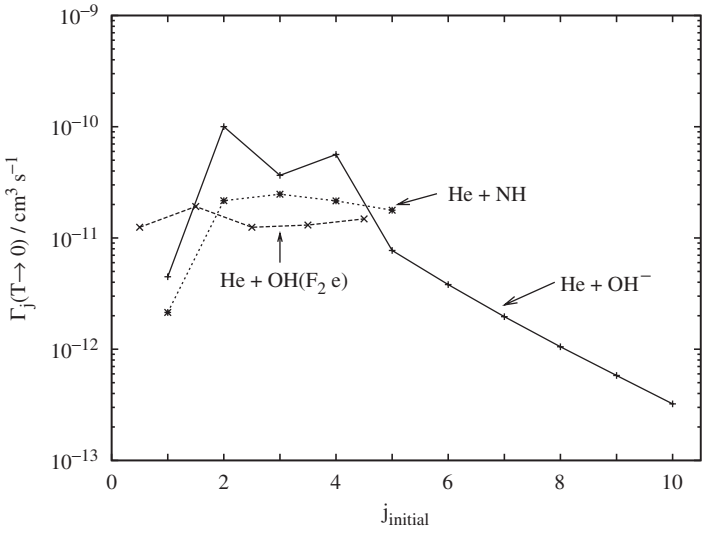

Figure 11. Rotational cooling rates at vanishing energies, as a function of the initial j state. Solid line: OH^-; dashes: OH target; short dashes: NH from [43]. Adapted from [80].

Table 1. Scattering lengths (Å) and rate constants (cm^3s^{-1}). Adapted from [81].

Initial j	α_j(Å)	β_j(Å)	$\Gamma_j(T\rightarrow 0)$
He_2^+-He			
2	−33.9	22.6	6.7e-10
4	+24.8	28.0	8.4e-10
6	−14.1	42.1	1.2e-09
Ne_2^+-Ne			
2	+371.6	55.5	3.3e-10
4	+103.6	124.5	7.3e-10
6	−256.7	117.9	7.0e-10

Table 2. Scattering lengths (in Å) and zero temperature rate coefficients (in cm^3s^{-1}) for the $OH^- + He$ system.

Initial j state	α_j	β_j	$\Gamma_j(T\rightarrow 0)$
1	32.61	0.1820	4.48(−12)
2	34.47	4.0677	1.00(−10)
3	32.60	1.4832	3.65(−11)
4	34.43	2.2877	5.63(−11)
5	31.88	0.3134	7.72(−12)
6	31.48	0.1546	3.81(−12)
7	31.28	0.7963	1.96(−12)
8	31.19	0.0427	1.05(−12)
9	31.14	0.0235	5.80(−13)
10	31.09	0.0131	3.22(−13)

whose values can be as large as 10^6 Å for the Ne_3^+ system. We note that the interactions in these systems are one order of magnitude larger than those which act in OH^--He. For direct comparison we report in table 2 the same set of data for the OH^-+He collision. As can be seen from the real parts of the scattering lengths, the elastic part of the scattering process is almost the same for He_2^+ and for OH^- because the isotropic long-range interaction responsible for its size is due to the polarizability of the He atom only. This behavior is further confirmed by the larger scattering lengths that we find for the Ne system where the polarizability of the atom is much larger.

The inelastic process is much less sensitive to the charge-polarization term and while in OH^--He is mainly driven by the long-range polarization-dipole term in equation (17), in the two homonuclear systems He_2^+ and Ne_2^+ is more likely due to the strong short-range coupling potential, a feature that is confirmed by an analysis of the state-to-state scattering cross-section: in the former system we have a clear dominance of the $\Delta j = 1$ transitions, while in the latter's also the transitions with $\Delta j > 2$ are important.

4. Vibrational quenching

Vibrational de-excitation processes are very important in the field of cold molecules because vibrational excited molecules appear in many experiments. As we have said

in the introduction, vibrationally excited molecules are the product of a photoassociation process or an association through a Feshbach resonance. The vibrational quenching that follows the formation of the molecule is the main source of loss of species in these experiments and normally cause the destruction of the cold molecules which have been produced. There exists however a notable exception: if the molecules, associated *via* a Feshbach resonance, come from a gas of fermionic atoms the resulting dimers which are now in their highest vibrational state, are stable against vibrational quenching for longer times (lifetimes are of the order of seconds); this effect being probably due to a phenomenon similar to Pauli blocking in fermion–fermion collisions [84–86] has allowed the creation of long-lived metastable molecular Bose–Einstein condensate [11–13]. This phenomenon however seems to be effective only for highly vibrationally excited molecule: in [34] it has been shown that for low initial vibrational states ($v \leq 3$), there is no systematic suppression of the quenching rates for molecules formed from fermionic atoms, even when the atom-atom scattering length is large and positive.

All these considerations are valid for molecules in their highest vibrationally excited states. It turns out, however, to be particularly difficult from the theoretical point view to explore those regimes, essentially for two reasons: the lack of properly calculated potential energy surfaces and the difficulties for traditional scattering codes to deal with many ro-vibrational states (for a Cs_2 molecule in its triplet states we can expect 50 vibrational levels and thousands of rotational states that have to be coupled).

On the other hand, a mild vibrational excitation might be expected in buffer gas cooling experiments where the decay of the population of $v \neq 0$ molecules can be detected and compared with calculations [42]. In this case the possibility of estimating the lifetime of vibrationally excited molecule in a buffer gas may also be important in view of subsequent trapping and evaporative cooling. There have been a notable number of works on vibrationally excited molecules in low vibrational states: Dalgarno and coworkers have examined the vibrational quenching in CO-He [87–89] from $v=1$ and 2 and in O_2+He [90]. Stoecklin *et al.* have investigated F_2 and N_2 and even N_2^+ molecules [91–93]. The present authors have instead investigated the behavior of highly polar molecules such as HF and LiH in comparison with CO [94]. We now summarize all these results together with a new calculation (which is presented here for the first time) by the present authors on the ionic system Li^++H_2.

4.1. *Quenching from low v states*

Vibrational quenching cross-sections are in general very small compared to rotational quenching cross-sections. This is due to the weak dependence of the interaction potential involving He as partner on the stretching of the molecular bond in comparison with the angular anisotropy. As an example we report in figure 12 the quenching rate for CO in the $v=1, j=0$ and $v=1, j=1$ levels as a function of temperature [87]. In the limit of zero energy, only the s-wave contributes and the rates approach the constant temperature dependence suggested by Wigner's law. As can be seen the transition which involves a pure rotational transition ($v=1, j=1 \rightarrow v=1, j=0$) is by orders of magnitude dominant over that involving a pure vibrational one.

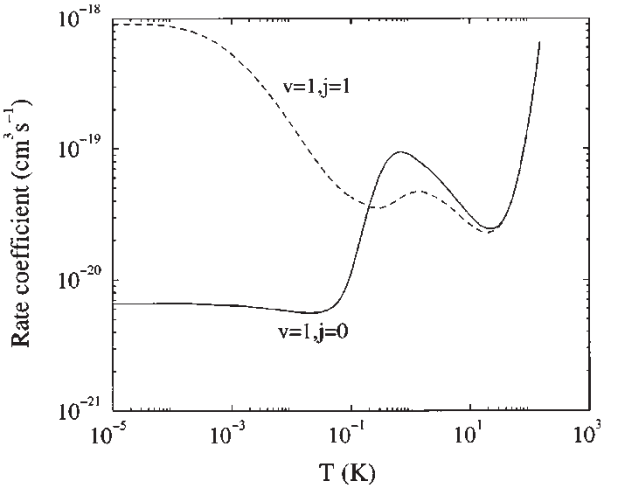

Figure 12. Rate coefficient for the quenching of the $v = 1, j = 0$ and $v = 1, j = 1$ levels of CO in collisions with ^{4}He as functions of the temperature. Adapted from [87].

A similar treatment of ^{3}He+O_2 [88] showed the same features although, given the stronger interaction due to the presence of the open-shell molecule, it showed a slightly larger rate constant for vibrational de-excitation. F_2 and N_2 were also studied in collision with ^{3}He by Stoecklin *et al.* in [91, 92] where the authors also provide two new accurate PESs. An interesting comparison between the PESs describing three homonuclear systems is provided in [92] from where we have taken the numbers reported here in table 3: the main difference between the three systems is that F_2 has a collinear absolute minimum geometry while N_2 and O_2 prefer a C_{2v} structure. Although the overall interactions are on the whole similar in well depth, some striking differences appear however in their scattering properties: the relevant scattering parameters for elastic and quenching processes are reported in table 4 where we show the imaginary part of the scattering lengths and the limiting value of the quenching rate constant for the three systems and for the few initial states which have been examined. The data reported in table 4 stress once again the large difference in magnitude for pure vibrational and ro-vibrational de-excitation processes. The unexpectedly very high value of the vibrational quenching rate attained in the case of F_2 with respect to N_2 is attributed by the authors to the specific feature of the PES involved through the use of a semiclassical model suggested recently by Nikitin *et al.* [95].

We have also analyzed in detail [94] the behavior of vibrational quenching in a small series of heteronuclear diatomics: CO, HF, and LiH. In order to attempt a comparison of the dynamical behavior of the three title systems a short analysis of their potential energy surfaces (PESs) is required. Two of the three PES's, CO + He [96] and HF + He [97] have been calculated using the Symmetry-Adapted Perturbation Theory (SAPT) method, while the LiH + He surface was obtained instead by using the MP2 method with a CCSD(T) correction [98]. In figure 13 we report the energy contours of the lowest adiabatic coupling element obtained from the PESs, namely the

Table 3. Comparison of the well depths and geometries of the He-O_2, He-N_2, and He-F_2 van der Waals complexes. R is the He-molecule distance, r is the molecular bond length. Adapted from [92].

Systems	R (a_0)	r (a_0)	D_e(cm^{-1})	Method
$N_2(0^\circ)$	7.50	2.0743	16.197	BCCD(T) [91]
$N_2(90^\circ)$	6.45	2.0743	21.711	BCCD(T) [91]
$O_2(0^\circ)$	6.90	2.282	25.613	CCSD(T) [78]
$O_2(90^\circ)$	6.00	2.282	27.895	CCSD(T) [78]
$F_2(0^\circ)$	6.50	2.668	37.53	BCCD(T) [92]
$F_2(90^\circ)$	5.65	2.668	32.72	BCCD(T) [92]

Table 4. Comparison of the imaginary part of the scattering length and quenching rates for He-O_2, He-N_2, and He-F_2 van der Waals complexes.

State (v, j)	β(Å)	$\Gamma(cm_3\,s^{-1})$
$N_2(1,0)$	9.98×10^{-9}	3×10^{-19} [91]
$N_2(0,2)$	2.677×10^{-1}	8×10^{-12} [91]
$O_2(1,1)$	1.8×10^{-7}	4×10^{-18} [88]
$O_2(0,3)$	3.94×10^{-1}	1.15×10^{-11} [88]
$F_2(1,0)$	2.89×10^{-3}	9.5×10^{-14} [92]

numerical results for the integral $\int_0^\infty \chi_0(r)V(r,R,\theta)\chi_0(r)dr$ that returns a $V_{00}(R,\theta)$ PES to be used in the dynamical calculations: for non-reactive systems such quantities are very similar to the rigid rotor interaction $V(r_{eq},R,\theta)$. In each of the panels the PES for values of R smaller than 2.0 Å is not shown: it is clear from the figure that the three systems have completely different interaction profiles: the CO surface (top panel) is almost isotropic and has a well depth of about $-20\,cm^{-1}$; the HF interaction is much less isotropic showing the presence of two similar wells of about $-35\,cm^{-1}$ at 0° and 90°; LiH-He surface, on the other hand, is very anisotropic. This is partly due to the large mass difference between lithium and hydrogen that places the LiH centre of mass (c.o.m) very close to the lithium atom, and partly because the LiH electronic structure resembles a Li^+H^- ion pair state with a very anisotropic electron density distribution. The potential well is also much deeper here and reaches $-180\,cm^{-1}$ on the Li side of the target.

The calculations have been performed over a wide range of collision energies (from 10^{-7} to $1\,cm^{-1}$) that includes the Wigner's law regime and energies at which the first shape resonances appear, a region that represents a situation in which the behavior of the cross-sections changes completely from the ultracold regime. The state-to-state ro-vibrational cross-sections from $v=2$ and $v=1$ have been calculated using a full CC approach and using both ^{3}He and ^{4}He. The s-wave elastic and inelastic cross-sections, determined at $10^{-7}\,cm^{-1}$, have been used to calculate the real and imaginary parts of the scattering length. The s-wave **S** matrix was then used to determine the sign of α. These and the other quantities described in the previous section are reported in table 5 (The results that we find here for the CO + He system are very similar to those

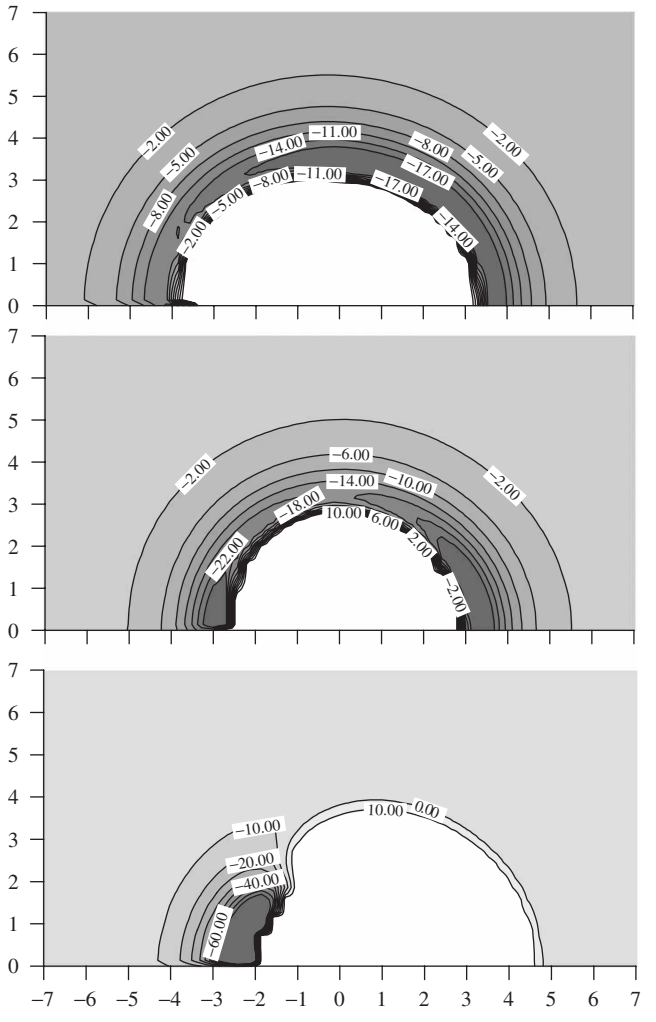

Figure 13. Energy contours for the V_{00} diagonal elements of the interaction potentials in cylindrical coordinates (the origin is located in the centre of mass of the molecule) for the three systems considered here: from top to bottom CO, HF, and LiH. Distances are in Å and energy levels in cm^{-1}. Adapted from [94].

reported in [87, 88] both for the scattering lengths and for the total quenching rates). Some of the scattering lengths turn out to be negative (bold numbers in table 5), and this means that some of the interaction potentials are not able to accommodate a true metastable state near threshold. The resulting computed energies E are thus those of a virtual state living on the non-physical Riemann sheet of the complex energy plane. At the same time the lifetimes of the collision complexes are marked as negative as it happens in electron–molecule scattering when a Ramsauer–Townsend effect takes place [99]. All the quantities reported in table 5 confirm that the LiH molecule is by far the one with the largest rate coefficient for the vibrational de-excitation

Table 5. Computed quantities from the s-wave cross-sections and S-matrix. See text for meaning of symbols. Adapted from [94].

System	α_v(Å)	β_v(Å)	E(cm^{-1})	τ(s)	$\Gamma_v(cm^3 \cdot s^{-1})$
$CO(v=2)+{}^3He$	3.9	7.3e − 9	−0.40	4.2e − 4	2.13e − 19
$CO(v=2)+{}^4He$	**−5.4**	5.7e − 10	**−0.17**	1.8e − 2	1.29e − 20
$CO(v=1)+{}^3He$	4.36	4.6e − 9	−0.31	4.1e − 3	1.3e − 19
$CO(v=1)+{}^4He$	**−4.87**	2.3e − 10	**−0.24**	1.0e − 1	5.3e − 21
$HF(v=2)+{}^3He$	1.8	8.5e − 5	−2.0	3.3e − 9	2.6e − 15
$HF(v=2)+{}^4He$	**−2.8**	2.7e − 4	**−0.62**	−5.4e − 9	6.5e − 15
$HF(v=1)+{}^3He$	1.7	1.0e − 5	−2.3	9.3e − 8	3.1e − 16
$HF(v=1)+{}^4He$	**−3.1**	3.4e − 5	**−0.51**	−2.4e − 7	8.1e − 16
$LiH(v=2)+{}^3He$	6.1	9.8e − 2	−0.20	9.9e − 11	3.6e − 12
$LiH(v=2)+{}^4He$	2.4	4.9e − 1	−0.95	1.6e − 12	1.5e − 11
$LiH(v=1)+{}^3He$	5.8	2.4e − 3	−0.22	1.4e − 8	9.0e − 14
$LiH(v=1)+{}^4He$	1.3	1.2e − 2	−3.44	4.0e − 11	3.8e − 13

and the one with the shortest lifetimes. The variations of polarity when going from C-O to Li-H reflect themselves rather clearly on the angular dependence (orientational anisotropy) variations exhibited by the three systems: only weakly dependent on θ in the case of CO-He while the dependence becomes markedly stronger for LiH-He: the interaction are therefore producing $\Delta v = 1$ relaxation cross-section limiting values for the LiH molecular partner which are about two or three orders of magnitude larger than in the case of HF and five to six orders of magnitude larger than for the CO molecule.

As an example we report in 14 the computed elastic and inelastic cross-sections due to the vibrational quenching collisions from the second excited vibrational state ($v=2$) of LiH. There are now two possible quenching processes during which the molecule can release its vibrational energy content: a two-quanta vibrational jump and a single quantum jump. In all the three systems the $\Delta v = 2$ jump is less efficient than the single quantum exchange as it should be expected for Van der Waals systems and from simple energy gap consideration (e.g. see [100]), but while the difference is only two orders of magnitude for HF, it goes up to four orders of magnitude for LiH and is even larger for CO (see a detailed discussion in [89]). This expected behavior can be explained in simple terms when considering the relative strength of the V_{01} and V_{02} vibrational coupling elements for all the three systems. For CO and LiH the total quenching rate for vibrational transition from $v=2$ are larger than those from the $v=1$ level (see the values of β in table 5) because the vibrational relaxation from higher levels is more efficient as expected from the reduction of the vibrational energy gap when going to excited states.

Some of the scattering lengths reported in table 5 have negative values (they are shown by bold face digits) and therefore the collisional systems for which this happens also exhibit in the elastic cross-sections marked Ramsauer minima. This point is rather interesting since another feature that makes LiH a good candidate for collisional cooling is also the absence of such minima in our calculations. They, in fact, might make the He buffer gas completely 'transparent' to molecules at some particular kinetic energy

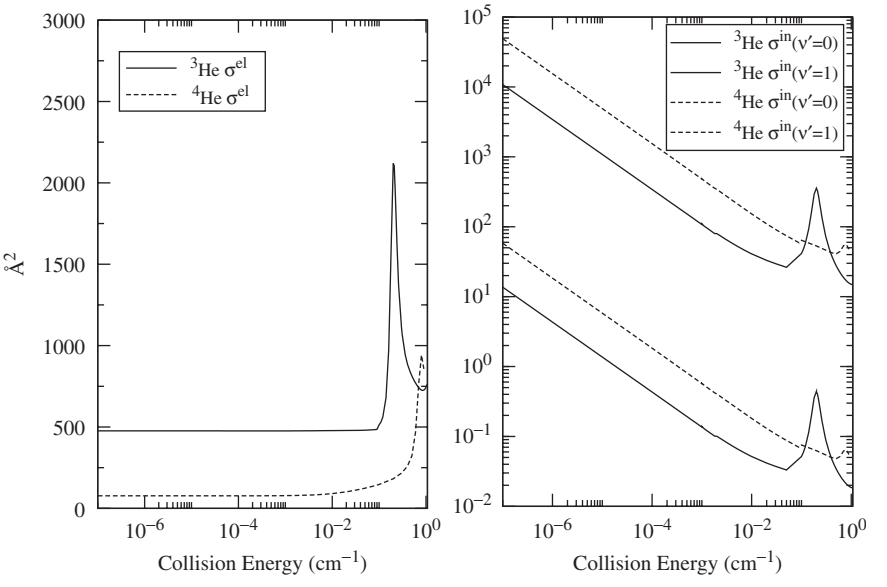

Figure 14. Vibrational quenching (right panel) and elastic (left panel) cross-section for LiH($v = 2$)+^{3}He and LiH($v = 2$)+^{4}He. Adapted from [94].

thereby reducing the efficiency at which these molecules thermalize with the chosen buffer gas.

Balkrishnan *et al*. have carried out quantum mechanical scattering calculations of elastic and ro-vibrationally inelastic transitions in CaH($^2\Sigma$) by collisions with ^{3}He atoms [42] and they provide a interesting comparison with the experimental results by [22]. Cross-sections for quenching of the $v = 1, N = 0$ level of the CaH molecule are shown in figure 15 as functions of the kinetic energy. The cross-section is dominated by a $l = 2$ shape resonance where the cross-section varies by about three orders of magnitude. The rate coefficient at zero temperature attains the finite limiting value of $2.6 \times 10^{-17}\,\mathrm{cm^3\,s^{-1}}$; it then increases by a factor of 50 because of the shape resonance shown in figure 15. The rate coefficient at 0.5 K is $6.4 \times 10^{-16}\,\mathrm{cm^3\,s^{-1}}$, only a factor of 6 larger than the experimental upper limit.

4.2. *Quenching from high v states*

As we have said before, apart from the buffer gas loading technique most molecules produced in photoassociation or through Feshbach resonances are vibrationally excited in their highest vibrational levels. However, the dynamics of vibrational quenching from highly excited states is still poorly understood and only two model calculations, as far as we know, have been published to date: one on the $H_2 + H$ system [62, 101] and another for the H_2+He system [63]. Additionally, exploratory computations have been performed for Li_3 [34] and K_3 [36].

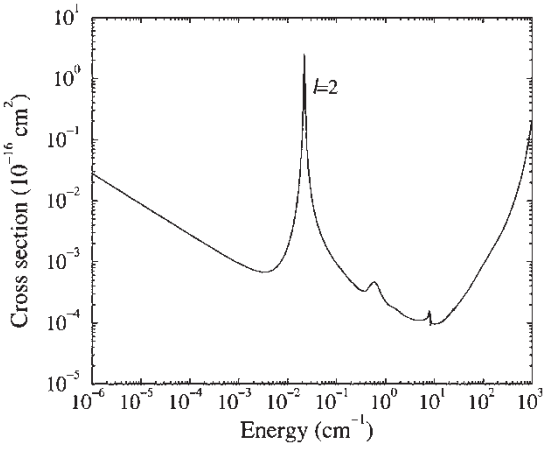

Figure 15. Cross-sections for quenching of the $v = 1, N = 0$ level of CaH by collisions with ^{3}He as functions of the incident kinetic energy. Adapted from [42].

In the former numerical experiments, Dalgarno and coworkers found that the vibrational quenching rate in the ultralow energy limit was strongly dependent on the initial vibrational level. As an example we report in figure 16 the total quenching rates from all the vibrational level of H_2 in collision with ^{3}He as presented in ref. [63]. As discussed in the introduction, two recent experiments by Weidemüller [37] and Pillet [38] have measured the rate of vibrational de-excitation for Cs_2 from highly vibrational states in collision with Cs atoms and found that the rates did not depend much upon the initial vibrational state of the molecule. Stimulated by such recent experiments, we have carried out an analysis of vibrational de-excitation processes for $Li_2(^1\Sigma_g^+)$ in collision with ^{4}He at ultralow energies as those that can exist in an optical trap. The choice of such a system is simply motivated by the fact that it has the computational advantage of not including any reactive channel (LiHe is not bound) and therefore we can correctly describe the collision process using the somewhat simpler dynamics of inelastic scattering only. In order to calculate the wavefunctions of the isolated Li_2 molecule, we have used the RKR potential available in the literature [102] with the long-range part of the potential obtained from [103]. This finally 'fused' form of the PES of Li_2 (for $J = 0$) supports 42 vibrational levels in close agreement with the ones reported by the above articles. We have further extended the previously calculated PES reported in [69] to include the explicit dependence of the interaction on the internal molecular coordinate producing the interaction potential over a range of r values for the Li_2 (2.1–15.0 Å) via QCISD(T) with a cc-pVQZ basis set. The resulting PES was then fitted analytically with the following method: we have generated the non-separable three-body interaction using the expression

$$V_{3B}(r_1, r_2, r_3) = V_{Li_2He}(r_1, r_2, r_3) - V_{Li_2}(r_1) - V_{LiHe}(r_2) - V_{LiHe}(r_3) \qquad (20)$$

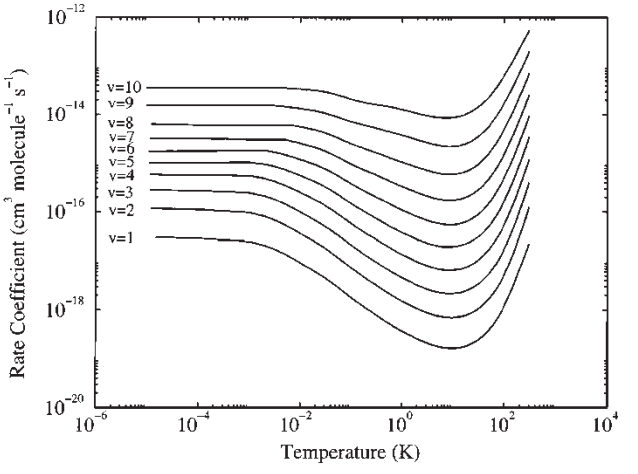

Figure 16. Total vibrational relaxation rate coefficients for the deactivation of H_2 in collisions with ^3He as a function of temperature for different vibrational levels of the molecule. Adapted from [63].

which has then been fitted using the Aguado–Paniagua type of expansion [104]. Our interaction potential is then constructed out of the sum of this three-body potential plus two accurate Li-He diatomic contributions that we have taken from [105].

The calculations have been done only for total angular momentum $J=0$ and for different initial vibrational states of the molecule up to $v=30$ in the rotational state $j=0$. We have included in the basis set all the 42 vibrational states of the isolated molecule and up to $j_{max}=48$. In the whole treatment we have neglected the coupling with the continuum of the Li_2 molecule. The results reported by figure 17 show the asymptotic behavior of the elastic and total quenching cross-section from the initial levels $v=30, 25, 20, 15, 10$. While the elastic cross-section is seen to be only weakly dependent on the initial v, the inelastic ones show instead a much more marked variation with v as it has been found in the earlier calculations of [63, 101] for the H_2 molecule and in contrast with experimental findings. We present a more complete view of the results in figure 18 where for each initial vibrational state we report both the total inelastic cross-section (scale on the left) and the limiting value of the corresponding rate constant (scale on the right).

In order to see the possible role played by the density of states (given the much larger number of vibrational levels supported by the triplet ground state of Cs_2) we have repeated the calculations for the non-reactive collision in Li_2-He increasing the density of states in the diatomic molecules by arbitrarily increasing the mass of the two Li atoms. In order to keep the calculation manageable we have included only the $j=0$ state for Li_2 (rotationless approximation).

The results of figure 19 in the panel on the left report the exact and rotationless inelastic total quenching cross-sections in the Li_2-He system obtained as in figure 6 and show the relatively small modifications due to the use of the rotationless approximation. The results of the panel on the right report the same

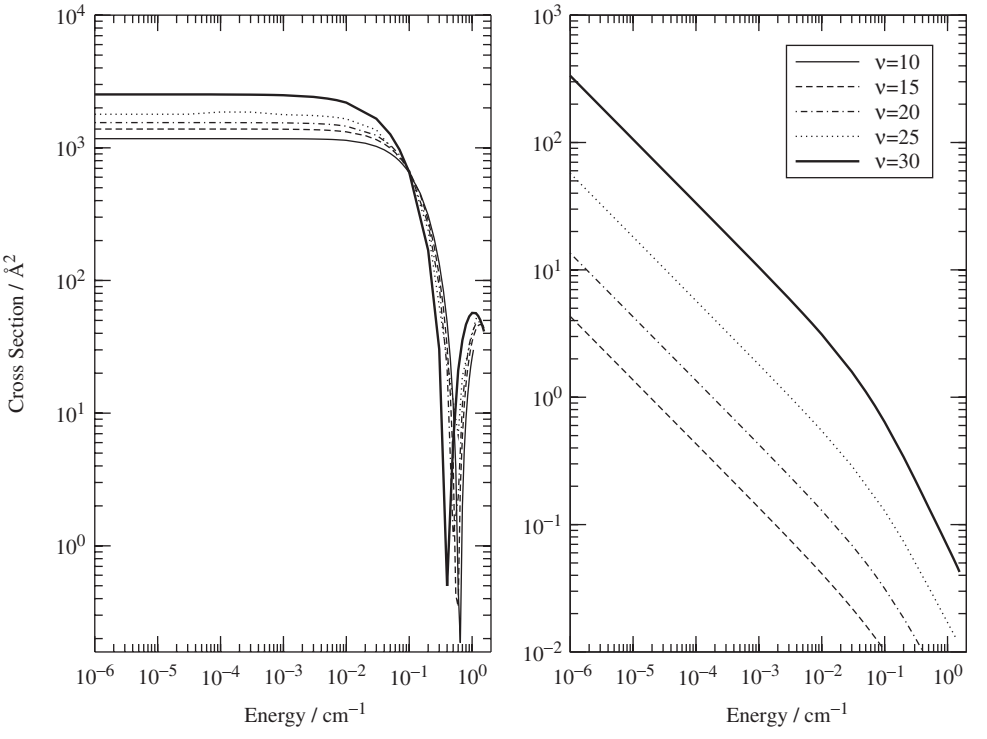

Figure 17. Computed elastic (left) and inelastic (right) cross-sections (in units of Å^2) as a function of collision energy values. Adapted from [106].

inelastic cross-sections when the diatomic mass is varied up to several sizes larger than the correct one. The calculations clearly indicates a flattening of its dependence on the initial vibrational level: we are now in a regime of 'level congestion' which is more similar to that existing in Cs_2 ($\omega_e \sim 20\,cm^{-1}$ for triplet Cs_2 and is $\sim 100\,cm^{-1}$ for the 'heaviest' Li_2). The goal of this numerical experiment was to help our understanding of the collisional quenching processes seen to occur in ultracold traps used in recent experiments [37, 38]: increasing the density of states of the diatoms in the above systems lead to a weaker dependence of the de-excitation cross-sections upon the initial vibrational state of the molecule and therefore shows a trend that is more similar to that seen by the experiments on vibrational de-excitation.

4.3. *Ionic systems: virtual state scattering*

Virtual-state scattering has been shown to be relevant for the scattering at ultralow energies both in atom–diatom reactive systems [39] and in electron–molecule scattering [99]. Stoecklin *et al.* [93] have considered the vibrational quenching of N_2^+ in the $v = 1, j = 0$ state colliding with ^{3}He and ^{4}He. This system was chosen because of the possibility of comparing the results with the neutral He-N_2 system [92]. When the differences between the quenching cross-section involving the two isotopes of

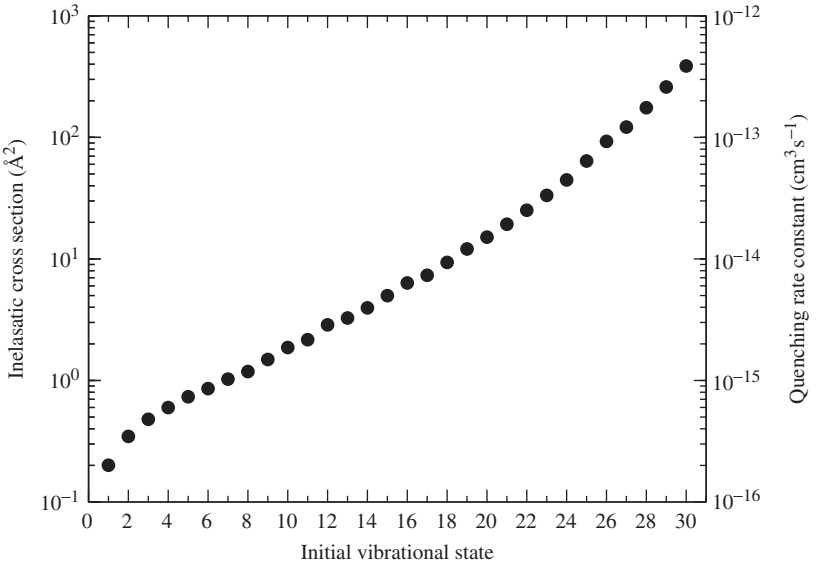

Figure 18. Computed total quenching cross-sections for $Li_2 + He$ as a function of the initial vibrational state. The scale on the right measures the corresponding $T = 0$ rate coefficient. Adapted from [106].

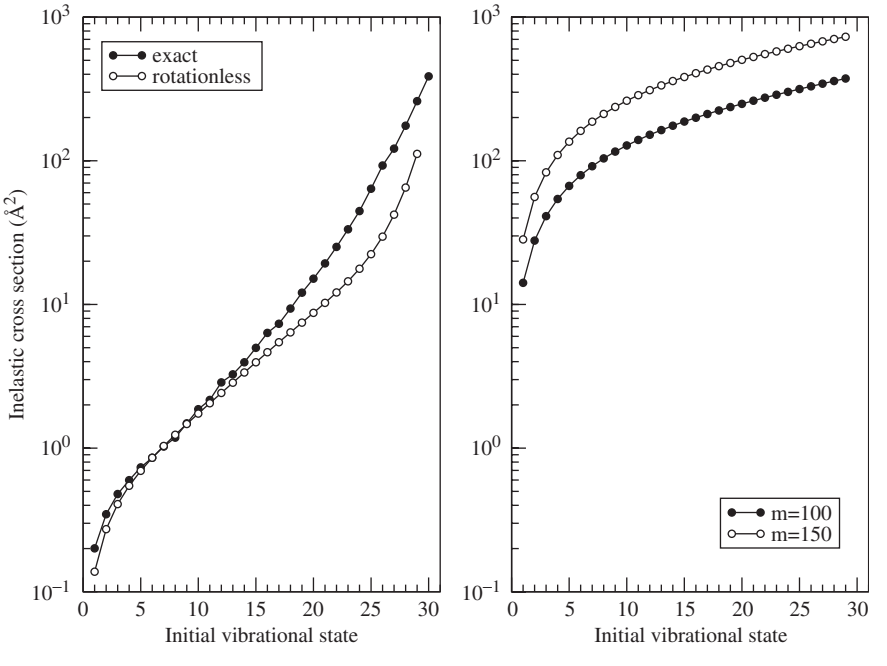

Figure 19. Computed total quenching cross-sections as a function of the initial vibrational state for $Li_2 + He$. Left panel: exact and rotationless approximation; right panel: large mass increase. Adapted from [106].

Table 6. Real and imaginary parts of the scattering lengths associated with the quenching of $N_2^+(v=1,j=0)$ and $N_2(v=1,j=0)$ in collision with the two isotopes of the helium atom. Adapted from [92].

	^{3}He-N_2^+	^{4}He-N_2^+	^{3}He-N_2	^{4}He-N_2
$\alpha(\mathring{A})$	−96.7	40.5	4.18	2.67
$\beta(\mathring{A})$	1.22×10^{-3}	1.4×10^{-4}	9.98×10^{-9}	1.93×10^{-8}

the helium atom is considered, one sees that, while they are not very strong in the case of the collision involving neutral N_2, there is a striking difference in the ionic case with N_2^+. As an example we report the relevant scattering lengths in table 6. The six orders of magnitude difference of the β values between the neutral N_2 and the ions is simply due to the fact that the potential well associated with the van der Waals complex becomes now much deeper in the case of the ionic species and because of the importance of the long-range charge induced dipole potential at very low kinetic energy. However, as the authors point out [93] the surprising difference is that found between the two isotopic variants for N_2^+ calculations. Such difference is too large to be due only to a mass effect: it is instead likely to be due to the fact that the two systems are characterized by two different scattering regimes: the one with ^{3}He is indeed in the virtual state scattering regime where the resonant interaction of the scattering wavefunction with a near-threshold virtual state (α is negative and large) can increase the probability of inelastic processes as previously noticed by Bodo *et al*. [39].

A very similar behavior has also been noticed by us in the analysis of the scattering between Li^+ and H_2 molecules. The potential energy surface has been presented in detail elsewhere [107–109] and its features will be only briefly analyzed here. The PES which we are interested in is the ground electronic state of the LiH_2^+ complex. The reaction that takes place over this adiabatic PES is

$$LiH^+ + H \longrightarrow Li^+ + H_2 \tag{21}$$

and is exoergic by about 4.4 eV due to the low binding energy of LiH^+ ($D_0 = 0.112$ eV) [109]. The PES shows a purely downhill route in going from LiH^+ to H_2 and has its absolute minima in C_{2v} geometry that is located 0.286 eV below the $H_2 + Li^+$ asymptote. Since we are mainly interested in the non-reactive scattering of Li^+ of H_2 molecules we neglect the reactive interaction which could lead to the formation of LiH^+ during an H-atom exchange reaction. Due to the large exothermicity of equation (27), in fact, a vibrationally excited hydrogen molecule in the eleventh state would be required for a low collision energy in order to make that reaction channel accessible. Here we will present cross-sections for the maximum vibrational level $v=3$.

The PES we have employed in the present work is expressed in Jacobi coordinates and presents a well of about 2300 cm^{-1} for a Li^+ approaching in C_{2v} geometry to

the H_2 molecule that reduces to $\sim 650\,cm^{-1}$ for collinear geometries. The interaction at long range is dominated by the multipolar terms due to the quadrupole and polarizability of H_2 [109] and is given by

$$V_{LR}(R, r, \theta) = \frac{Q(H_2)P_2(\cos(\theta))}{R^3} - \frac{\alpha_0(H_2)}{2R^4} - \frac{\alpha_2(H_2)P_2(\cos(\theta))}{2R^4} \tag{22}$$

where R is the distance of the lithium atom from the centre of the H_2 moiety, r is the H-H distance, θ is the Jacobi angle, Q and α_i are the quadrupole and the anisotropic polarizabilities of the H_2 molecule. Angular cuts through this PES are reported in figure 20.

The rotationally summed cross-sections for three different initial vibrational states of the H_2 molecule are reported in figure 21 together with the elastic cross-sections (on the right) [110]. We can see that the transitions from $v=1$ and $v=3$ have a similar shape and the expected relative size (see the discussion for CO at the beginning of this section), while the quenching from $v=2$ has a very different shape with a broad 'hump' superimposed on a linear dependence appearing at very low energies ($\sim 4 \times 10^{-4}\,cm^{-1}$) and due to the $l=1$ component. Moreover its value seems to be too small with respect the the other two cross-sections. This is exactly the same situation that Stoecklin *et al*. encountered in the $N_2^+ + He$ system discussed previously [93]: while in their case, the parameter that was determining the scattering regime was the mass of the He atom, here it is the initial state of the molecule. If one therefore looks at the scattering lengths that we report in table 7, one sees how we have again an effect due to virtual state scattering occurring in this system. The Van der Waals complexes $Li^+ \cdots H_2(v, j=0)$ with $v=1$ and 3 support a metastable virtual state near

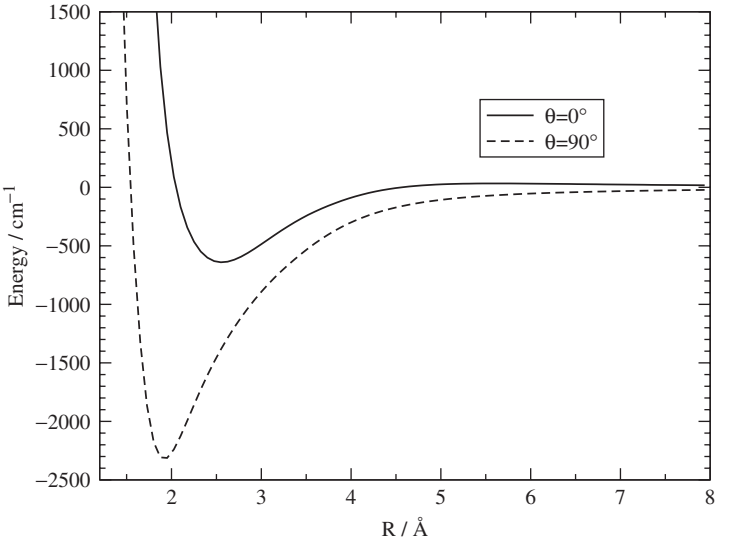

Figure 20. Angular cuts of the Li^+-H_2 PES. Data from [109].

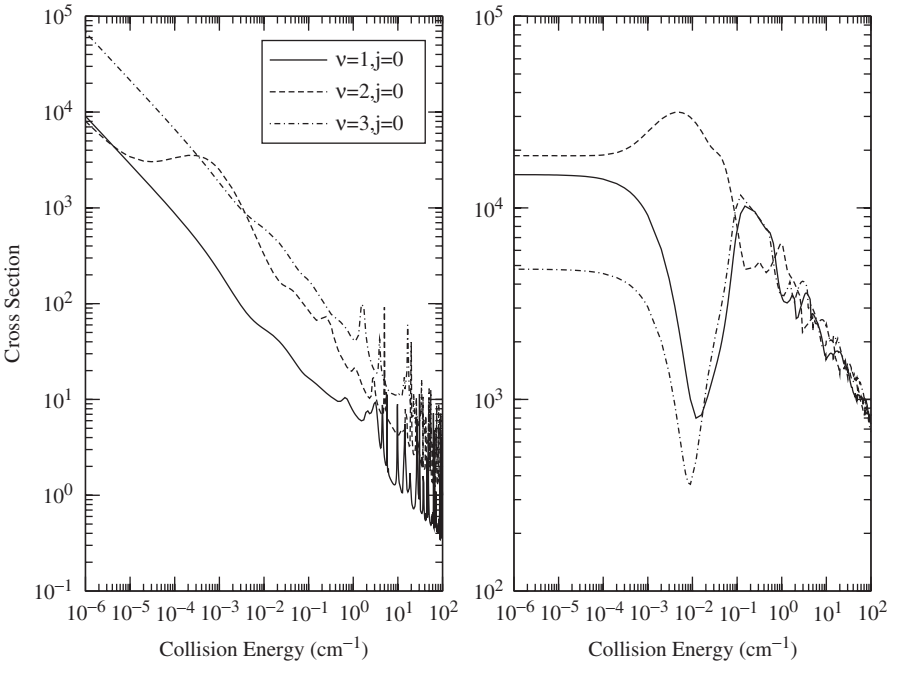

Figure 21. Quenching (left) and elastic (right) cross-sections for $Li^+ + H_2(v = 1, 2, 3, j = 0)$. Adapted from [110].

Table 7. Real and imaginary parts of the scattering lengths associated with the quenching of $Li^+ + H_2(v = 1,2,3, j = 0)$.

	$v = 1$	$v = 2$	$v = 3$
$\alpha(\mathring{A})$	−34.60	38.60	−19.46
$\beta(\mathring{A})$	0.22	0.18	1.65

the dissociation threshold which has a enhancing effect on the inelastic scattering cross-sections (negative α). The metastability of the virtual states in this case is due to the fact that the coupling to the continuum of the $Li^+ \cdots H_2(v = 0, j = 0)$ makes its lifetime finite in the same way as in the case of a resonance. The lifetimes can be calculated and turns out to be 20 and 0.5 ns respectively for $v = 1$ and 3.

By comparing the behavior of the $Li^+ + H_2$ and $N_2^+ + He$ systems we can see that virtual state scattering is a common situation especially in ionic systems and that it should have an important role in determining scattering regimes that can be tuned through the use of external fields [17] which in turn could provide a useful tool for controlling ultracold chemistry processes [39, 111].

5. Present conclusions

The variety of examples and the amount of work presented in this review testifies to the tremendous increase which has occurred in the last few years to the theoretical and computational interest on the accurate studies of the quantum treatments of collisions at ultralow energies. Such an interest has been naturally spurred by the outstanding growth of the experimental findings which has also occurred at the same time and by the dissemination over many laboratories around the world of the very sophisticated tools which are needed to handle this class of collisional experiments. As a consequence of such experimental variety of data, which we have tried to summarize in the present review, the corresponding computations have needed to progress along at least two pathways: (i) the assembly of highly correlated and reliable potential energy surfaces which can describe the weak interactions between helium atoms and neutral molecular partners and (ii) the more complex handling of the angular momenta coupling schemes which act during the ultralow energy collisions and which require correct knowledge of smaller terms of the relevant Hamiltonians like spin–orbit and spin–spin contributions.

Furthermore, the presence of ionic molecules has also been considered and the marked difference implied by the presence of a different class of long-range forces have also been discussed and produced by the calculations. The special features related to 'quantum suppression', i.e. the reduced phase interference which occurs at ultralow energies which are dominated by only few angular momenta (and, eventually, only by s-wave scattering processes) are also interestingly presented by the quenching behavior of the various molecular partners analyzed in this review: small features of the interaction potentials are seen, in fact, to be able to become amplified as very marked differences in the behavior of the scattering attributes (e.g. scattering lengths, inelastic cross-sections, virtual state locations, etc.) and therefore are suggested to be amenable of experimental detection.

In summary, the field of quantum scattering of ultracold molecular systems is a rapidly growing area of theoretical chemical physics and an area which this review intends to accurately represent at this point in time.

Acknowledgments

We thank the University of Rome 'La Sapienza' Research Committee, the CASPUR Supercomputing Consortium, the 'Cold Molecules Network' n. HPRN-CT-2002-00290 and the PRIN2004 Research Project for financial and computational support.

References

[1] B. G. Levi, Phys. Today **53,** 46 (2000).
[2] L. H. Bethlem, G. Berden, F. M. H. Crompvoets, R. T. Jongma, A. J. A. van Roij, and G. Meijer, Nature **406,** 491 (2000).
[3] R. Wynar, R. S. Freeland, D. J. Han, C. Ryu, and D. J. Heinzen, Science **287,** 1016 (2000).

[4] K. Xu, T. Makaiyama, J. R. Abo-Shaeer, J. K. Chin, D. E. Miller, and W. Ketterle, Phys. Rev. Lett. **91,** 210402 (2003).
[5] K. E. Strecker, G. B. Partridge, and R. G. Hulet, Phys. Rev. Lett. **91,** 080406 (2003).
[6] H. L. Bethlem and G. Meijer, Int. Rev. Phys. Chem. **22,** 73 (2003).
[7] J. Doyle, B. Friedrich, R. V. Krems, and F. Masnou-Seeuws, Eur. Phys. J. D **31,** 149 (2004).
[8] F. M. H. Crompvoets, R. T. Jongma, H. L. Bethlem, A. J. A. van Roij, and G. Meijer, Phys. Rev. Lett. **89,** 093004 (2002).
[9] D. Egorov, T. Lahaye, W. Schöllkopf, B. Friedrich, and J. M. Doyle., Phys. Rev. A **66,** 043401 (2002).
[10] J. Herbig, T. Kraemer, M. Mark, T. Weber, C. Chin, H.-C. Nägerl, and R. Grimm, Science **301,** 1510 (2003).
[11] M. Greiner, C. A. Regal, and D. S. Jin, Nature **426,** 537 (2003).
[12] S. Jochim, M. Bartenstein, A. Altmeyer, G. Hendl, S. Riedl, C. Chin, J. D. Denshlag, and R. Grimm, Science **302,** 2101 (2003).
[13] M. W. Zwierlein, C. A. Stan, C. H. Schunck, S. M. F. Raupach, S. Gupta, Z. Hadzibabic, and W. Ketterle, Phys. Rev. Lett. **91,** 250401 (2003).
[14] T. Mukaiyama, J. R. Abo-Shaeer, K. Xu, J. K. Chin, and W. Ketterle, Phys. Rev. Lett. **92,** 180402 (2004).
[15] C. Chin, T. Kraemer, M. Mark, J. Herbig, P. Waldburger, H.-C. Nägerl, and R. Grimm, Phys. Rev. Lett. **94,** 123201 (2005).
[16] R. Grimm, Nature **435,** 1035 (2005).
[17] R. V. Krems, Int. Rev. Phys. Chem. **24,** 99 (2005).
[18] J. M. Doyle, B. Friedrich, J. Kim, and D. Patterson, Phys. Rev. A **52** R2515 (1995).
[19] J. Weinstein, R. deCarvalho, T. Guillet, B. Friedrich, and J. M. Doyle, Nature **395,** 148 (1998).
[20] S. Y. T. van de Meerakker, N. Vanhaecke, H. L. Bethlem, and G. Meijer, Phys. Rev. A **73,** 023401 (2006).
[21] S. Y. T. van de Meerakker, P. H. M. Smeets, N. Vanhaecke, R. T. Jongma, and G. Meijer, Phys. Rev. Lett. **94,** 023004 (2005).
[22] J. D. Weinstein, PhD thesis, Harvard University (2001).
[23] D. Egorov, J. D. Weinstein, D. Patterson, B. Friedrich, and J. M. Doyle, Phys. Rev. A **63,** 030501 (2001).
[24] D. Egorov, W. C. Campbell, B. Friedrich, S. E. Maxwell, E. Tsikata, L. D. van Buuren, and J. M. Doyle, Eur. Phys. J. D **31,** 307 (2004).
[25] D. M. Egorov, PhD thesis, Harvard University (2004).
[26] K. Maussang, D. Egorov, J. Helton, S. Nguyen, and J. Doyle, Phys. Rev. Lett. **94,** 123002 (2004).
[27] J. Bahns, W. Stwalley, and P. Gould, Adv. At. Mol. Opt. Phys. **42,** 171 (2000).
[28] F. Masnou-Seeuws and P. Pillet, Adv. At. Mol. Opt. Phys. **47,** 53 (2001).
[29] W. Stwalley and H. Wang, J. Mol. Spectrosc. **195,** 194 (1999).
[30] R. C. Forrey, V. Kharchenko, N. Balakrishnan, and A. Dalgarno, Phys. Rev. A **59,** 2146 (1999a).
[31] H. Wang and W. C. Stwalley, J. Chem. Phys. **108,** 5767 (1998).
[32] P. Soldán, M. T. Cvitaš, and J. M. Hutson, Phys. Rev. A **67** eid054702 (2003).
[33] P. Soldán, M. T. Cvitaš, J. M. Hutson, P. Honvault, and J.-M. Launay, Phys. Rev. Lett. **89,** 153201 (2002).
[34] M. T. Cvitaš, P. Soldán, J. M. Hutson, P. Honvault, and J.-M. Launay, Phys. Rev. Lett. **94** 033201 (2005a).
[35] M. T. Cvitaš, P. Soldán, J. M. Hutson, P. Honvault, and J.-M. Launay, Phys. Rev. Lett. **94,** 200402 (2005b).
[36] G. Quéméner, P. Honvault, J.-M. Launay, P. Soldán, D. E. Potter, and J. M. Hutson, Phys. Rev. A **71,** 032722 (2005).
[37] P. Staanum, S. D. Kraft, J. Lange, R. Wester, and M. Weidemüller, Phys. Rev. Lett. **96,** 023201 (2006).
[38] N. Zahzam, T. Vogt, M. Mudrich, D. Comparat, and P. Pillet, Phys. Rev. Lett. **96,** 023202 (2006).
[39] E. Bodo, N. Balkrishnan, A. Dalgarno, and F. A. Gianturco, J. Phys. B **37,** 3641 (2004a).
[40] G. Meijer and G. C. Groenenboom, private communication (2006).
[41] R. V. Krems and A. Dalgarno, J. Chem. Phys. **120,** 2296 (2004).
[42] N. Balakrishnan, G. C. Groenenboom, R. V. Krems, and A. Dalgarno, J. Chem. Phys. **118,** 7386 (2003).
[43] R. Krems, A. Dalgarno, N. Balakrishnan, and G. C. Groenenboom, Phys. Rev. A **67,** 060703 (2003a).
[44] M. Drewsen, I. Jensen, J. Lindballe, N. Nissen, R. Martinussen, A. Mortensen, P. Staanum, and D. Voigt, Int. J. of Mass Spectrometry **229,** 89 (2003).
[45] M. A. van Eijkelenborg, M. E. M. Storkey, D. M. Segal, and R. C. Thompson, Phys. Rev. A **60,** 3903 (1999).
[46] I. S. Vogelius, L. B. Madsen, and M. Drewsen, Phys. Rev. A **70,** 053412 (2004).

[47] P. Blythe, B. Roth, U. Fröhlich, H. Wenz, and S. Schiller, Phys. Rev. Lett. **95,** 183002 (2005).
[48] S. Jørgensen, M. Drewsen, and R. Kosloff, J. Chem. Phys. **123,** 094302 (2005).
[49] H. R. Sadeghpour, J. L. Bohn, M. J. Cavagnero, B. D. Esry, I. I. Fabrikant, J. H. Macek, and A. R. P. Rau, J. Phys. B **33** R93 (2000).
[50] D. DeMille, Phys. Rev. Lett. **88,** 067901 (2002).
[51] A. M. Arthurs and A. Dalgarno, Proc. R. Soc. **256,** 540 (1960).
[52] M. H. Alexander, J. Chem. Phys. **76,** 3637 (1982).
[53] G. C. Corey and M. H. Alexander, J. Chem. Phys. **85,** 5652 (1986).
[54] P. J. Dagdigian, M. H. Alexander, and K. Liu, J. Chem. Phys. **91,** 839 (1986).
[55] D. E. Manolopoulos, J. Chem. Phys. **85,** 6425 (1986).
[56] A. Degasperis, Il Nuovo Cimento **XXXIV**, 1667 (1964).
[57] R. Martinazzo, E. Bodo, and F. A. Gianturco, Comp. Phys. Comm. **151,** 187 (2003a).
[58] A. V. Avdeenkov and J. L. Bohn, Phys. Rev. A **64,** 052703 (2001).
[59] J. L. Bohn, Phys. Rev. A **63,** 052714 (2001).
[60] A. V. Avdeenkov and J. L. Bohn, Phys. Rev. A **66,** 052718 (2002).
[61] P. E. Wigner, Phys. Rev. **73,** 1002 (1948).
[62] N. Balakrishnan, V. Kharchenko, R. C. Forrey, and A. Dalgarno, Chem. Phys. Lett. **280,** 5 (1997a).
[63] N. Balakrishnan, R. C. Forrey, and A. Dalgarno, Phys. Rev. Lett. **80,** 3224 (1998).
[64] P. H. G. Quéméner and J.-M. Launay, Eur. Phys. J. D **30,** 201 (2004).
[65] R. C. Forrey, Phys. Rev. A **63,** 051403 (2001).
[66] R. C. Forrey, Phys. Rev. A **66,** 023411 (2002).
[67] R. C. Forrey, N. Balakrishnan, and A. Dalgarno, Phys. Rev. Lett. **82,** 2657 (1999b).
[68] R. C. Forrey, Eur. Phys. J. D **31,** 409 (2004).
[69] E. Bodo, F. A. Gianturco, F. Sebastianelli, E. Yurtsever, and M. Yurtsever, Theor. Chem. Acc. **112,** 263 (2004b).
[70] E. Bodo, F. Sebastianelli, F. A. Gianturco, E. Yurtsever, and M. Yurtsever, J. Chem. Phys. **120,** 9160 (2004c).
[71] K. Tilford, M. Hoster, P. M. Florian, and R. C. Forrey, Phys. Rev. A **69,** 052705 (2004).
[72] G. Meijer, Chem. Phys. Chem. **3,** 495 (2002).
[73] L. Gonzalez-Sanchez, E. Bodo, and F. A. Gianturco, Phys. Rev. A **73,** 032702 (2006a).
[74] R. V. Krems, H. R. Sadeghpour, A. Dalgarno, D. Zgid, J. Klos, and G. Chalasinski, Phys. Rev. A **68,** 051401 (2003b).
[75] F. Marinetti, E. Bodo, and F. A. Gianturco, J. Theor. Comp. Chem. Accepted.
[76] authorH.-Sung, A. M. Coy, R. Toczylowski, and S. Cybulski, J. Chem. Phys. **113,** 5736 (2000).
[77] S. F. Boys and F. Bernardi, Mol. Phys. **19,** 553 (1970).
[78] G. C. Groenenboom and I. M. Struniewicz, J. Chem. Phys. **113,** 9562 (2000).
[79] R. Ahlrichs, H. J. Bohm, S. Brode, K. T. Tang, and J. P. Toennies, J. Chem. Phys. **88,** 6290 (1987).
[80] L. Gonzalez-Sanchez, F. Marinetti, E. Bodo, and F. A. Gianturco, J. Phys. B (in press) (2006b).
[81] E. Bodo, E. Scifoni, F. Sebastianelli, F. Gianturco, and A. Dalgarno, Phys. Rev. Lett. **89,** (2002a).
[82] F. A. Gianturco and F. Sebastianelli, Eur. Phys. J. D **10,** 399 (2000).
[83] F. Sebastianelli, F. A. Gianturco, and E. Yurtsever, Int. J. Mass Spectr. **220,** 193 (2002).
[84] D. S. Petrov, Phys. Rev. A **67,** 010703 (2003).
[85] D. S. Petrov, C. Salomon, and G. V. Shlyapnikov, Phys. Rev. Lett. **93,** 090404 (2004).
[86] D. S. Petrov, C. Salomon, and G. V. Shlyapnikov, Phys. Rev. A **71,** 012708 (2005).
[87] N. Balakrishnan, A. Dalgarno, and R. C. Forrey, J. Chem. Phys. **113,** 621 (2000).
[88] C. Zhu, N. Balakrishnan, and A. Dalgarno, J. Chem. Phys. **115,** 1335 (2001).
[89] E. Bodo, F. A. Gianturco, and A. Dalgarno, Chem. Phys. Lett. **353,** 1 (2002b).
[90] N. Balakrishnan and A. Dalgarno, J. Phys. Chem. A **105,** 2348 (2001).
[91] T. Stoecklin, A. Vorovin, and J. C. Rayez, Phys. Rev. A **66,** 042703 (2002).
[92] T. Stoecklin, A. Vorovin, and J. C. Rayez, Phys. Rev. A **68,** 032716 (2003).
[93] T. Stoecklin and A. Voronin, Phys. Rev. A **72,** 042714 (2005).
[94] E. Bodo and F. A. Gianturco, J. Phys. Chem. A **107,** 7328 (2003).
[95] E. I. Dashevskaya, J. A. Kunc, E. E. Nikitin, and I. Oref, J. Chem. Phys. **118,** 3141 (2003).
[96] T. G. Heijmen, R. Moszynski, P. Wormer, and A. van der Avoird, J. Chem. Phys. **107,** 9921 (1997).
[97] R. Moszynski, P. E. Wormer, B. Jeziorski, and A. van der Avoird, J. Chem. Phys. **101,** 2811 (1994).
[98] B. K. Taylor and R. J. Hinde, J. Chem. Phys. **111,** 973 (1999).
[99] D. Field and L. B. Masden, J. Chem. Phys. **118,** 1679 (2003).
[100] F. A. Gianturco, in *Collision Theory of Atoms and Molecules* (Plenum Publ. Co., 1989).

[101] N. Balakrishnan, R. Forrey, and A. Dalgarno, Chem. Phys. Lett. **280,** 1 (1997b).
[102] B. Barakat, R. Bacis, E. Carrot, S. Churrassy, P. Crozet, and F. Martin, Chem. Phys. **102,** 215 (1986).
[103] R. Cat, A. Dalgarno, and M. Jamieson, Phys. Rev. A **50,** 399 (1994).
[104] A. Aguado, C. Tablero, and M. Paniagua, Comp. Phys. Comm. **108,** 259 (1998).
[105] K. T. T. U. Kleinekathofer, J. P. Toennies, and C. L. Yiu, Chem. Phys. Lett. **249,** 257 (1996).
[106] E. Bodo, F. A. Gianturco, and E. Yurtsever, Phys. Rev. A **73,** 052715 (2006).
[107] E. Bodo, F. A. Gianturco, and R. Martinazzo, Chem. Phys. **271,** 309 (2001).
[108] R. Martinazzo, E. Bodo, F. A. Gianturco, and M. Raimondi, Chem. Phys. **287,** 335 (2003b).
[109] R. Martinazzo, G. F. Tantardini, E. Bodo, and F. A. Gianturco, J. Chem. Phys. **119,** 11241 (2003c).
[110] E. Bodo and F. A. Gianturco, submitted (2006).
[111] R. V. Krems, Phys. Rev. Lett. **96,** 123202 (2006).